CHALMERS
UNIVERSITY OF TECHNOLOGY

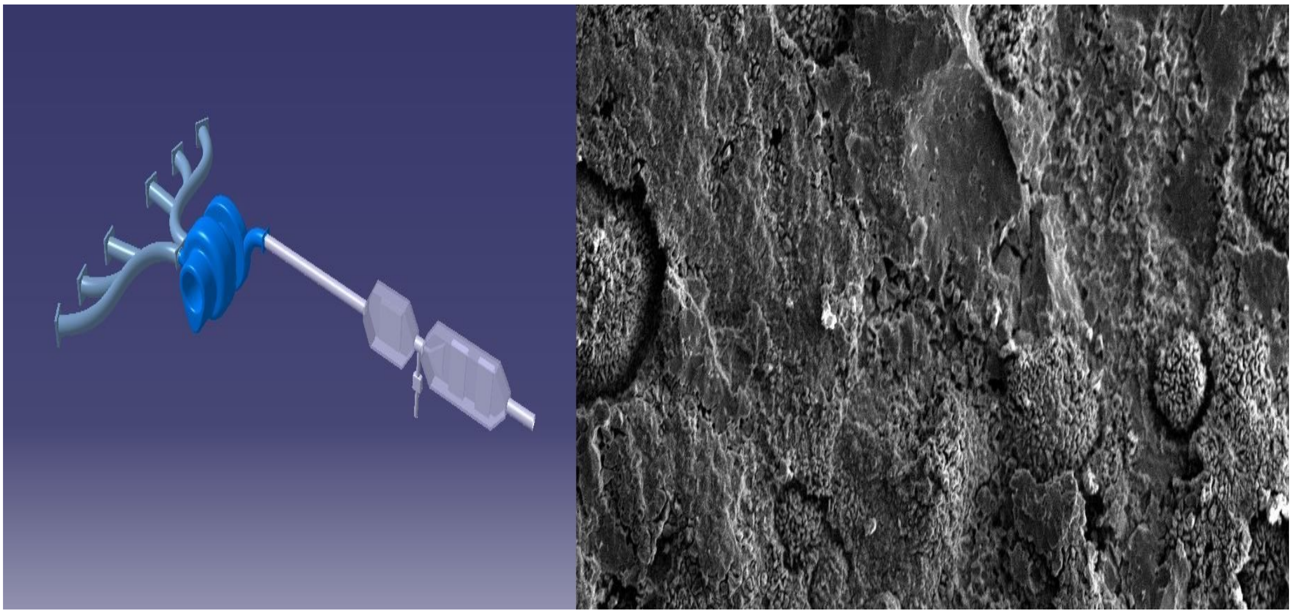

High temperature corrosion at urea dosage in heavy-duty trucks

Master's thesis in Materials Engineering

PRANESH UDHAYAKUMAR

Department of Chemistry and Chemical Engineering
Chalmers University of Technology
SE-412 96 Gothenburg,Sweden 2020

Master's thesis 2020

High temperature corrosion at urea dosage in heavy-duty trucks

PRANESH UDHAYAKUMAR

Department of Chemistry and Chemical Engineering
Chalmers University of Technology
SE-412 96 Gothenburg,Sweden 2020

High temperature corrosion at urea dosage in heavy-duty trucks
PRANESH UDHAYAKUMAR

© PRANESH UDHAYAKUMAR, 2020.

Supervisors

- Ragna Elger - Materials Technology, Power train (YTMN), SCANIA CV AB,SE-151 48 Södertälje,Sweden.
- Andrea Olivas - Department of Corrosion, Metallic materials in corrosive environment,SWERIM AB,SE-164 07 Kista,Sweden.

Examiner

Jesper Liske - High temperature corrosion centre, Department of Chemistry and Chemical Engineering,Centre of Excellence for High Temperature Corrosion (HTC), Chalmers University of Technology,SE-412 96,Sweden.

Cover:Simple 3D CATIA V5 model of a exhaust system of a heavy-duty truck diesel engine and SEM image of SiMo51 sample exposed in simulated exhaust gas atmosphere with 5%O_2+10%CO_2+10%H_2O+N_2+1%NH_3 at 700°C for 168h.

Master's Thesis 2020
Department of Chemistry and Chemical Engineering
Chalmers University of Technology
SE-412 96 Gothenburg
Telephone +46 31 772 1000

High temperature corrosion at urea dosage in heavy-duty trucks
PRANESH UDHAYAKUMAR
Department of Chemistry and Chemical Engineering
Chalmers University of Technology

Abstract

Increasing strict norms of emission control for automotive makes the manufacturers to reduce the unwanted emissions.This can be possible by improving the engine efficiency which eventually increases the engine operating temperature particularly in exhaust line where the higher temperature may lead to varying thermal load on the materials of the exhaust line.The increase in temperature may gradually increase the concentration of NOx as well.However,to reduce NOx emission from heavy duty trucks can be done by the most promising technology called selective catalytic reduction,a state-of-the-art technique which is being used in the exhaust system of the truck.Aqueous solution of urea (32.5% of Urea and 67.5% of water) is injected into the SCR system to reduce the NOx into nitrogen,water and oxygen by reduction reaction.But in this thesis work urea is not used whereas the ammonia is used in the simulated gas.As mentioned earlier,when the material is exposed to exhaust gas mixture (with urea) and higher operating temperature in exhaust line may have a severe effect on the materials used in terms of material degradation like lowering the mechanical properties, spallation into the downstream of the engine which is a very serious issue.The currently used SiMo51 for exhaust manifold and 1.4509 for silencer are showing certain drawbacks such as lacking reliable behaviour in higher temperatures over a long thermal load cycles and material degradation.In this study,different materials are exposed in the simulated exhaust gas atmosphere at 700°C and 550°C for 168h.Two atmospheres were used ,one as without ammonia (taken as a reference) and the other with ammonia (aqueous urea).Both ferritic and austenitic grade materials of wrought and cast group were used.Corrosion resistant behavior of stainless steels are complicated with oxygen and water present together in the environment.The materials developed iron rich oxide and Cr rich oxide on the surface, but some materials developed internal oxidation which might degrade the mechanical properties of a material as discussed earlier.

Keywords: High Temperature Corrosion,Ammonia,Austenitic and Ferritic Stainless Steel,Exhaust after-treatment,Oxidation,Nirtiding.

Acknowledgements

Firstly,I would like to thank my supervisors Ragna Elger,Mercedes Andrea Olivas Ogaz and Associate professor Jesper Liske for giving me this opportunity to work in this project,as they took time off from their busy schedule to constantly encourage and support me with their ardent guidance throughout the master thesis work,I quote a Chinese proverb,“giving a man a fish would feed him only for a day but if you teach him how to fish then you feed him for lifetime”.I sincerely thank them for their unlimited patience in guiding me and teaching me how to fish and grow further.

I thank FFI,Scania CV AB and Swerim AB for supporting and funding this project.In addition,I thank Outokumpu for providing me the materials for the project.Thanks to Rikard Norling and Alice Moya Núñez for their help in setting up the furnace also I thank Anders Thiblin for his detailed introduction of SEM/EDS,which was the most important part of my thesis work.

Special thanks to my friends Prakadesh Palanisamy,Shri Adithyan,Sudharsan Santhakumar,Tanuj Kattamanchi,Dharun Velmani Thanga Ratnam,Nandhini Kumaraswamy and Priya Murugeshan for their moral support throughout my masters and always cheering up when I am down.Finally,I would like to thank my parents and family back in India for their continuous support and guidance throughout my life.

Pranesh Udhayakumar,Gothenburg,October 2020

Contents

List of Figures

List of Tables

1

Introduction

Sweden's environmental goals are in accordance with the action of European Union.To reduce harmful emissions like PM,CO,NO_x etc from Automotive[1].With regard to that today the transport industry across the globe undergoes transition to provide sustainable transport system which protects society and environment from being polluted with the emissions like NO_x,CO,HC, SO_x etc.This makes the heavy duty truck manufacturers to produce trucks with high output efficiency which reduces the use of fuel.The high output efficiency means high operating conditions, which ends in a high temperature in the silencer.Indeed,the will to reduce NO_x emission through Euro 5 (2009) and then to Euro 6 (2014) and American EPA Tier 4 (2008-2015) gives the implementation of a new after-treatment system in the exhaust line [2].Accordingly to reduce NO_x in the silencer,Urea is dosed at high temperature.The urea dosage to reduce the NO_x emission at high temperature causes corrosive environment with oxidation and possible nitridation which could cause material wastage.An increase in operating temperature will make the materials in the silencer to face a new challenge regarding high temperature corrosion[3].

The exhaust system of heavy duty diesel engines undergo highly corrosive environment with O_2,H_2O,CO_2,NO_x etc at a cyclic environment and this challenges the currently used 1.4509 which is a ferritic stainless steel alloyed with carbon,chromium,low silicon and manganese content [4].An alternate material is needed to overcome the high temperature corrosion effects at urea dosage in order to avoid the material wastage and improve the materials behaviour in corrosive environment.

1.1 Objective and Research outline

This master thesis project is a part of Master's degree in Materials engineering at Chalmers University of Technology, Gothenburg,Sweden and was carried out in Materials technology department, Scania CV AB at Södertälje,Sweden and Swerim AB at Kista,Sweden.

The aim of the project is to analyse the material behaviour in synthetic gas with NH_3 at high temperature.The materials focused are wrought and cast materials with one nickel base,four ferritic and four austenitic stainless steels in corrosive environments at high temperature.The isothermal environment contains exhaust gas N_2,5%O_2,10%CO_2 and 10%H_2O with exposure time 168 hours,which will act as a reference exposure.Materials will be exposed to isothermal environment at the temperature of 700°C and 550°C with the mixture of 1%NH_3 and 5%O_2+10%CO_2+10%H_2O+N_2 of exhaust gases mentioned above for 168 hours,the mass change was then calculated at the end of the exposure time based on SS ISO 21608:2012(E)[5].The morphology and formed oxide thickness will be studied using Scanning Electron Microscopy(SEM),elements composition with Energy-dispersive X-ray Spectroscopy (EDS) and the phases of the oxide layer formed will be characterized using X-ray diffraction(XRD).

The nitridation of the stainless steels with increasing Nickel content is to be studied in the high temperature ammonia environment which may increase the alloy nitridation resistance[6].The most commonly used alloy SiMo51, a ferritic cast stainless steel for ammonia bearing high temperature environment,HK30,1.4509 and 1.4307 were investigated and also compared with other candidate materials.The possibility to obtain the resistance towards nitride formation on the surface or formation of internal nitrides will be possibly analysed according to[7].This project work is aimed to provide a new insight about the nitridation behaviour of wrought and cast stainless steels in a synthetic exhaust gas with presence of ammonia similar to the atmosphere in exhaust after treatment.

2

Background

2.1 Exhaust system of heavy-duty trucks

An automotive exhaust system is generally a piping assembly used to safely carry the burnt gases of combustion process away from the engine chamber.It is common for both Spark Ignition (SI) and Compression Ignition (CI) engines.The exhaust system contain main parts such as exhaust manifold,silencer,catalytic converters as shown in the figure 2.1.This study aims to analyse the material behaviour in silencer which is an acoustic component used to reduce the loudness and sound pressure from high temperature burning exhaust gases from the engine and also acts as the source of back pressure.The resonators are used inside the silencer in order to reduce the noise level. [8] particularly exhaust gas after-treatment system is present inside the silencer.

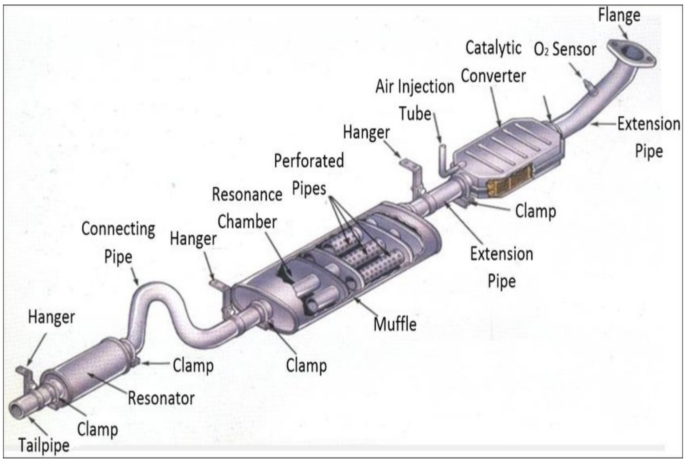

Figure 2.1: Typical view of an automotive exhaust system with its parts [9]

Today,according to Sweden environmental objective[1],emission norms by European Union has forced the automotive manufacturers to reduce the NO_x emissions from the exhaust line.The NO_x emission is controlled by using catalytic converter placed after the engine.There are different types of selective catalytic converters used based on the type of vehicle and Lean NO_x Trap (LNT),the latter is not present in all vehicles.Nowadays,Selective Catalytic Reduction (SCR) is the most common system for heavy duty trucks to reduce the NO_x according to Saghi Saedlou (see[2]).This selective catalytic converter reduces NO_x using ammonia (see[2]).As exhaust gases pass over the SCR catalyst,chemical reaction occur to reduce NO_x into nitrogen and water in equation 2.6.

The SCR set up is very often combined with a Particulate Filter (PF) for combined reductions of both Particulate Matter(PM) and Nitrogen oxide (NO_x) (see[2]). SCR injects Adblue,as shown in the fig 2.3,which is a source of ammonia,through a catalyst into the exhaust system of the engine (see figure2.2 and 2.3).Injection of Adblue reacts with NO_x and reduces its percentage.The AdBlue (aqueous solution of 37.5% of highly pure urea as per ISO 22241) is used according to European Commission and Joint Research Centre,2013.

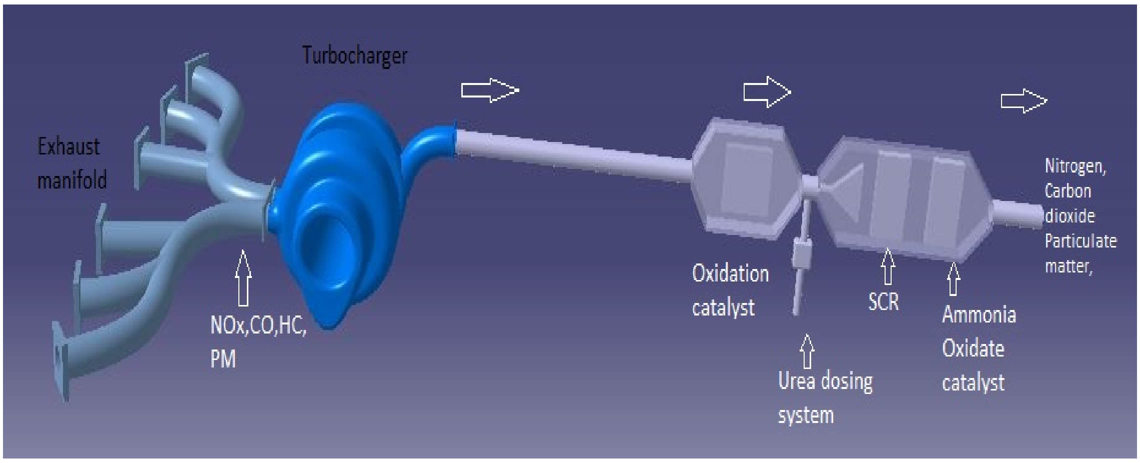

Figure 2.2: A simple sketch of exhaust system using CATIA V5

Ammonia reacts withNO_xin the catalyst at the temperature of 600°C. (see[7]) with the catalyst.There are few factors on which the reduction efficiency depends.They are temperature of the exhaust line,amount of urea injected,injection grid design and catalyst activity.By using the catalysts like V_2O/TiO_2[10] could be used in the SCR.

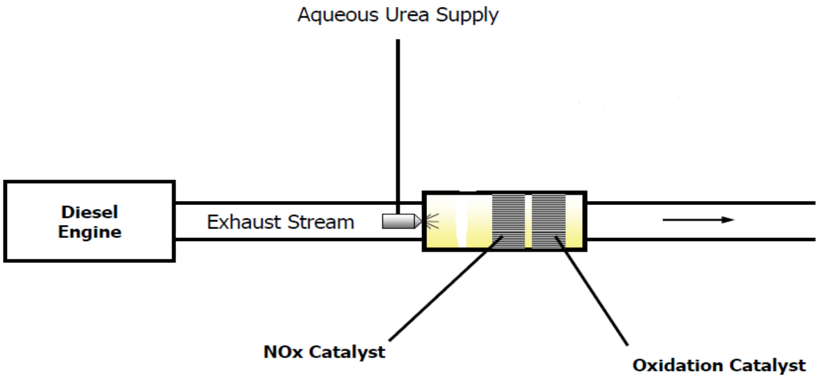

Figure 2.3: Schematic view of NO_x after treatment in SCR (Source -Cummins solutions)

$$\mathrm{NH_2CONH_{2(aq)}} \xrightarrow{>150°C} \mathrm{NH_{3(g)}} + \mathrm{HCNO_{(g)}} \tag{2.1}$$

$$\mathrm{HCNO}_{(ad)} + \mathrm{H_20} \xrightarrow{catalyst} \mathrm{NH}_{3(ad)} + \mathrm{CO}_{2(g)} \tag{2.2}$$

Ammonia generation by urea decomposition shown in equation 2.1 and equation 2.2 is according to Saedlou, S., Santacreu, P. and Leseux, J., 2011([2]) .

$$2\,\mathrm{NH_3} + \mathrm{NO} + \mathrm{NO_2} \longrightarrow 2\,\mathrm{N_2} + 3\,\mathrm{H_2O} \tag{2.3}$$

$$4\,\mathrm{NH_3} + 2\,\mathrm{NO_2} + \mathrm{O_2} \longrightarrow 2\,\mathrm{N_2} + 3\,\mathrm{H_2O} \tag{2.4}$$

$$4\,\mathrm{NH_3} + 4\,\mathrm{NO} + \mathrm{O_2} \longrightarrow 4\,\mathrm{N_2} + 6\,\mathrm{H_2O} \tag{2.5}$$

The above equation equation 2.3,2.4 and 2.5 show the NO_x reduction by ammonia on catalyst and equation equation 2.6 gives the global reaction[2].

$$\mathrm{(NH_2)_2CO} \xrightarrow{heat} \mathrm{NH_3} + \mathrm{NO}_x \xrightarrow{catalyst} \mathrm{N_2} + CO_2 + H_2O \tag{2.6}$$

The catalyst is made of metals and ceramics with porous structure,usually with honeycomb structure for ceramics and pleated for metals.The physical properties, composition and type of catalyst may affect the reliability and also new designs could increase the catalyst activity and the temperature range of reduction reaction[11].The catalyst activity is correlated with the NO_x reduction reaction rate.It is a function of factors such as mass transfer rate,gas temperature and gas composition.

- Thermal sintering of active sites due to high temperature in the exhaust system[11].

which might reduce the life time of the catalyst used.When the catalytic activity is reduced then the NO_x reduction is decreased.The different byproducts which deposits on the walls of silencer will decompose in high temperature and thus,the formed deposits reduce the function of the catalyst and also affects the corrosion behaviour of the exhaust system[12].

2.1.1 Working conditions of diesel engine

The selection of the type of exhaust after treatment depends on the engine operating condition.It may vary according to the manufacturer and the models.But the most common parameters are,

- higher fuel injection pressure,
- precise control of injection timing and rate including multi stage injection,
- optimization of fuel spray and air motion characteristics, centralized injection,
- higher levels of exhaust gas re-circulation (EGR),
- speed of the vehicle,
- position of the cylinders
- cylinder bore dimensions

The above mentioned factors may influence the engine working conditions and the fuel consumption[13],the diesel engine operation parameters may depend on speed,torque,load,fuel consumption rate,exhaust gas temperature and energy of exhaust gas[14] and these working conditions may influence the combustion and emission characteristics[15].The figure 2.4 shows that when the speed is at 1000

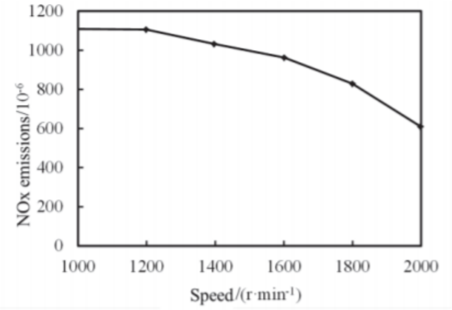

Figure 2.4: NO_x curve for diesel engine external load characteristics[15]

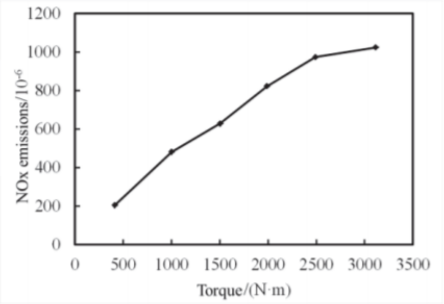

Figure 2.5: NO_x emission of the engine with the load at 1499r/min[14]

r/min,the NO_x emission concentration is higher and the NO_x emission concentration is reduced at the speed of 2000 r/min in the study done by Sun Zhixin for heavy duty diesel engines.NO_x emissions could decrease with increase in speed,specifically when the speed increases,the time for the diesel engine to complete a work cycle is shortened,accordingly the duration of combustion process is reduced,which make the stay time of the working fluid in the cylinder at high temperature reduced.But the stay time of the working fluid at the cylinder in high temperature will be an important factor to form NO_x[15].

The figure 2.5 gives the NO_x emission of the engine with the load at 1400 r/min.The NO_x emission of diesel engine increases with increase in load.When the load increases,the concentration of NO_x emission also rises.This increase in NO_x is because that increase in the load,the fuel supply of diesel engine keeps increasing,the combustion temperature in cylinder becomes more and stay time of the working fluid in high temperature becomes prolonged,which cause the increase of NO_x emissions.According to Sun Zhixin.,[14] at the lower speed external characteristics of the engine,cylinder pressure and temperature is low in the compression end point.And also when the fuel injection pressure is lower,there may be low quality of fuel atomization which end in prolonged delay of time,high combustion temperature and NO_x emissions.So at heavy load condition,because of the increased fuel supply,the combustion duration is longer,the combustion temperature higher and NO_x emissions are heavier.

2.1.2 Definition of High temperature corrosion

After the reduction reaction of NO_x in the catalytic converter,nitriding mechanism might occur due to Ammonia atmosphere in the high temperature corrosive environment of silencer (see[2]).Because of contact between exhaust gas products and hot stainless steel surface nitirides may form.The different behaviours of austenitic,ferritic stainless steel grades are studied by Saedlou.S et.al (see[2]).Finally, the exhaust gas flows to the tail pipe then to the atmosphere.

At high temperature environment,the corrosion occurs due to reaction of metal directly the atmosphere.When the steel is exposed to oxygen at room temperature or higher temperature,it may form protective oxide.The inherent property of the oxide scale may slow down the oxidation rate.The tendency to form an oxide is the important criteria for the corrosion of a metal in gaseous environment[16].There are other reactions like nitridation,oxidation,carburization,chlorination which depends on the atmosphere where the material is exposed.

2.1.3 Oxidation

Oxidation is the most important high temperature corrosion reaction.Alloys are oxidized when heated to elevated temperatures in air or in highly oxidizing environments such as combustion atmospheres with excess air or oxygen.

Ferrous alloys could be used for high temperature corrosion applications like automotive,bio reactors,aerospace etc.Io order to be able to form the corrosion resistance,the materials should be alloyed with elements like chromium,silicon, aluminium to form the protective oxide layer on the surface as mentioned in the previous section.These elements oxidize and form a protective barrier which protects the material from further corrosion.When a compact oxide scale formed on a metal surface is thin,and continuous,it might act as a protective oxide layer,preventing the inward and outward diffusion and thereby reducing the oxidation rate.The considerable amount of manganese may aid the formation of protective oxide layer to prevent further oxidation and acts as a corrosion resistance.The scale's condition is used to predict the high temperature corrosion resistance of a material.Factors which govern the scale are growth rate,adherence to the bulk material and porosity.Some cases also show another interesting mechanism called,breakaway oxidation.In certain cases,a phenomenon called breakaway oxidation will occur.Here,the scale finally loses its ability as a diffusion barrier.

When oxide layer spalls off,a new oxide layer called healing layer will form below which will prevent further degradation of the oxide scale.When the forming rate of healing layer is not fast enough then,non-protective oxides may form causing the oxidation through the bulk material.The content of alloying protective elements will influence thermodynamics of formation of the healing layer.For chromia forming materials,when the concentration of chromium in the metal/oxide scale interface is lower than the one of equilibrium with chromia,the forming of healing layer is not certain which ultimately form non-protective oxides,so called the phenomenon of breakaway oxidation[24].

Col.A et.al exposed austenitic stainless steel 304L in high temperature conditions with a temperature of 850°C in pure oxygen for 312 hours to investigate breakaway oxidation.The internal oxidation was studied which depends on the composition of the above healing layer.Preferential oxidation sites at the center of the grains,where the chromium flux towards the oxidation layer is less in order to form a protective chromia healing layer[25].

When oxide scale has a high defect density or when one of the oxide's sublattices contains a high degree of vacancies,the oxidation reactions can continue to proceed as linear oxide growth.With the effect of alloy depletion (probably chromium depletion) together with thick oxide scale formation which are susceptible to cracking and oxide scale spallation.Therefore,the formation of a protective oxide scale is more important for exhaust manifolds with oxidation protection[17].

The main criteria of the metal corrosion in the gaseous environment could be the ability of forming oxide scales which have negative free energy formation[18].

$$\mathrm{M(s)} + \mathrm{O_2(g)} \longrightarrow \mathrm{MO_2(s)} \tag{2.7}$$

Equation 2.7 shows the reaction of metal with oxygen to form a metal oxide MO_2. The free energy ΔG° should be negative in order to form the oxide MO_2.The obtained free energy could be compared to the oxygen partial pressure by using equilibrium condition,ΔG°-> RTlnpO2 where pO2 is the oxygen partial pressure,T is the temperature and R is a gas constant.By this equation,the dissociation pressure of oxygen with respect to any temperature can be obtained and also stability of oxides of different metals.These are well illustrated in the Ellígham's diagram[18]. The minimum partial pressure required for a metal to oxidize is calculated by ellígham's diagram (see fig 2.6) with the scale plotting ΔG° and Temperature T.The diagram shows whether the metal can be oxidized at the given temperature with the oxygen pressure.The reaction rate can not be predicted using this diagram.

2.1.3.1 Oxidation of Stainless steels

Stainless steel is a iron based alloy,where Cr concentration is more than 11.5%.These type of steels does not stain when exposed to wet environment by forming forming a thin passive layer of chromium oxide,which makes this as stainless steels.There are different ferritic and austenitic stainless steels available in the market.Most of the stainless steels are used for high temperature applications.Even though,ferritic stainless steels are good for many moderate temperature applications,their use is restricted for temperature capability[18].Ferritic stainless steels have the limit of maintaining high strength above 600 ∘ C as shown in the figure 2.7 below.But when increasing the C could increase the mechanical properties,while adding N the strength at low temperatures could be raised (according to The European Stainless Steel Development Association).

In regard to this drawback,austenitic grades are used.An austenitic phase is usually considered as a high temperature phase which are stable at room temperatures because of Ni or Mn.The most commonly used austenitic stainless steel is 304L with the chemical composition of 18% of Cr and 8% of Ni.For longer high temperature oxidation durability,the above mentioned Cr percentage is not enough so higher concentration of Cr is feasible to form a prolonged protective oxide scale.

2.1.4 Nitridation

Corrosion of stainless steel with Cr-Ni is more challenging when there are more than one oxidant in the environment.Nitridation occurs when the stainless steel or alloys are exposed to Nitrogen containing environment at high temperatures.Nitridation can cause the alloy to be embrtilled which is not recommended for long service period of the components,especially in the automotive exhaust line.

Scales formed during oxidation of chromium in air consist of an inner layer with Cr_2N and an outer layer of Cr_2O_7.Porosity has rarely been observed in the

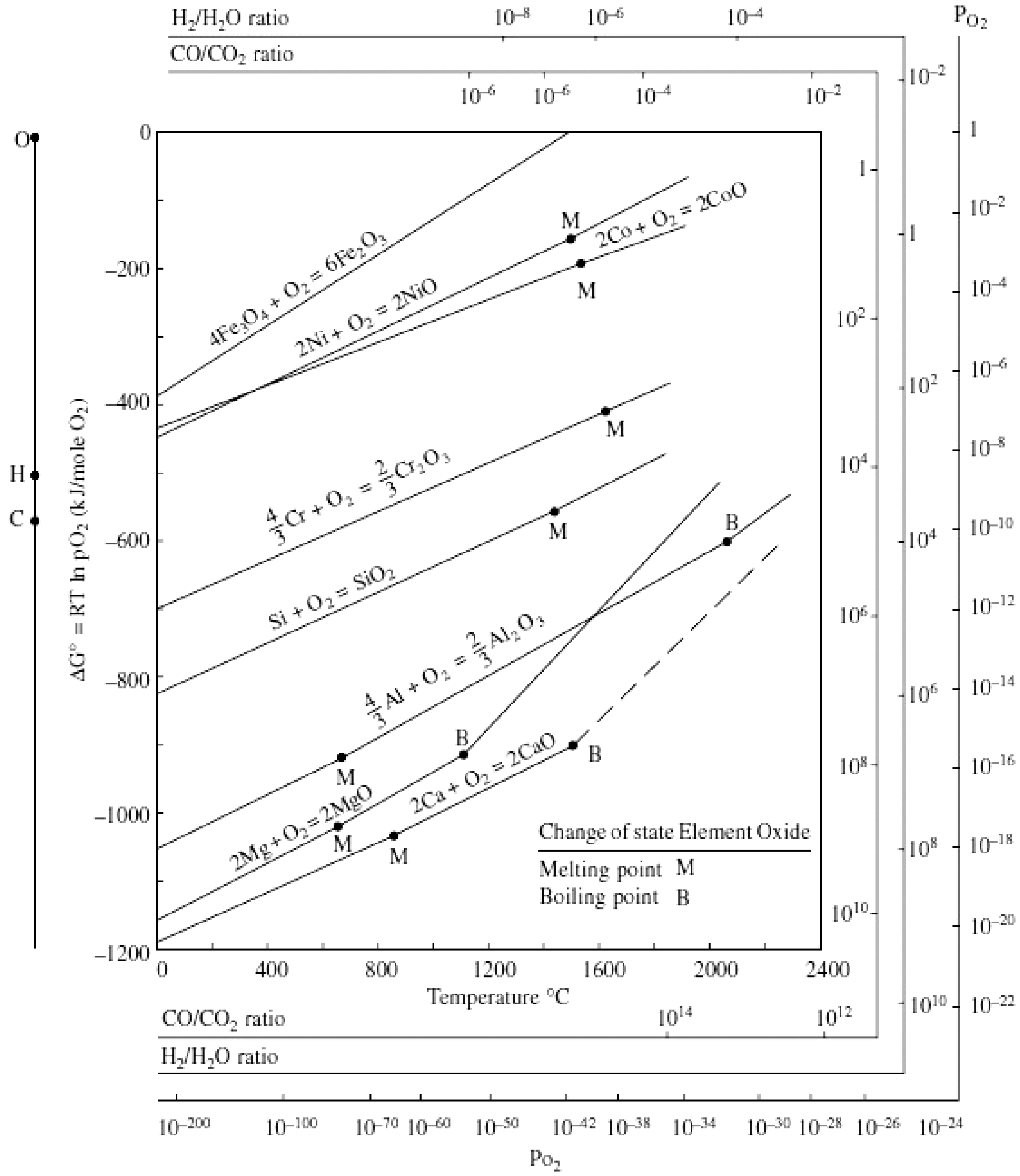

Figure 2.6: Elligham's diagram[18]

outer scale,the factor which is considered to be the cause for nitrogen penetration towards the metal/oxide scale interface.As nitrogen has lower chemical affinity for chromium than oxygen,it reacts with chromium at the metal/oxide interface,where the oxygen potential is less.And also the solubility of the Nitrogen in ferritic crystal structure is low,so that it has better performance than austenitic grades.There are different scaling reaction for chromium and chromia forming alloys with respect to the composition of gas.Varied scale morphologies and oxidation kinetics are observed in the presence and absence of water vapor depending on oxygen partial pressure.The additional presence of N_2 in the reactive gas leads to the formation of Cr_2N.Figure below shows the formation of Cr_2N under the Chromia scale[19].

Excessive formation of nitrides at the surface of cast materials might result in depletion of oxide-forming element like Cr which eventually reduce the oxidation

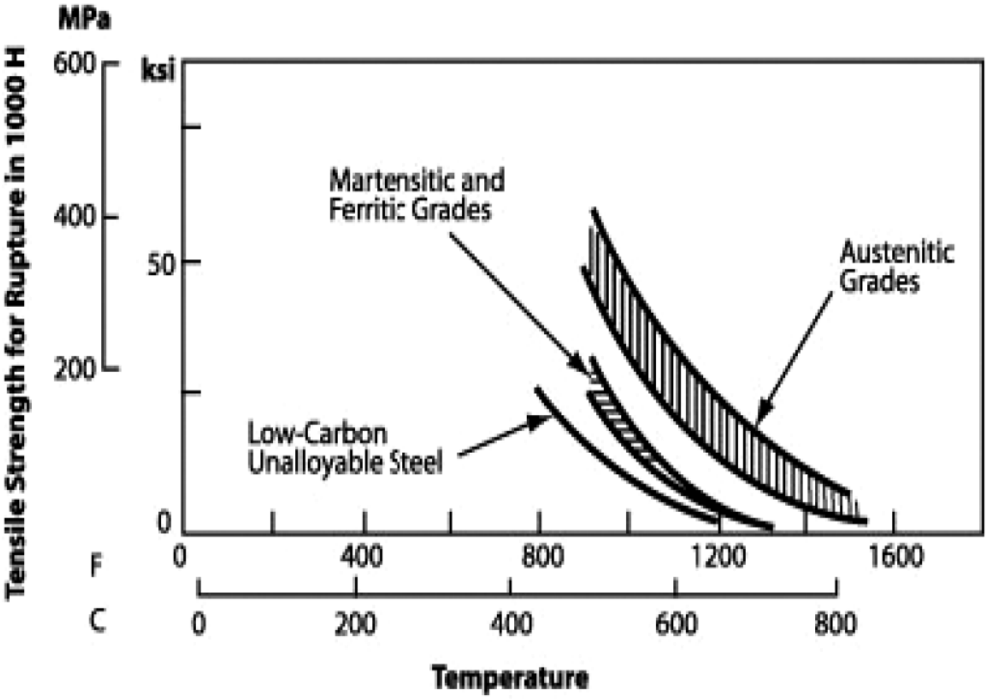

Figure 2.7: Comparing tensile stregnth of stainless steels with other steels[18]

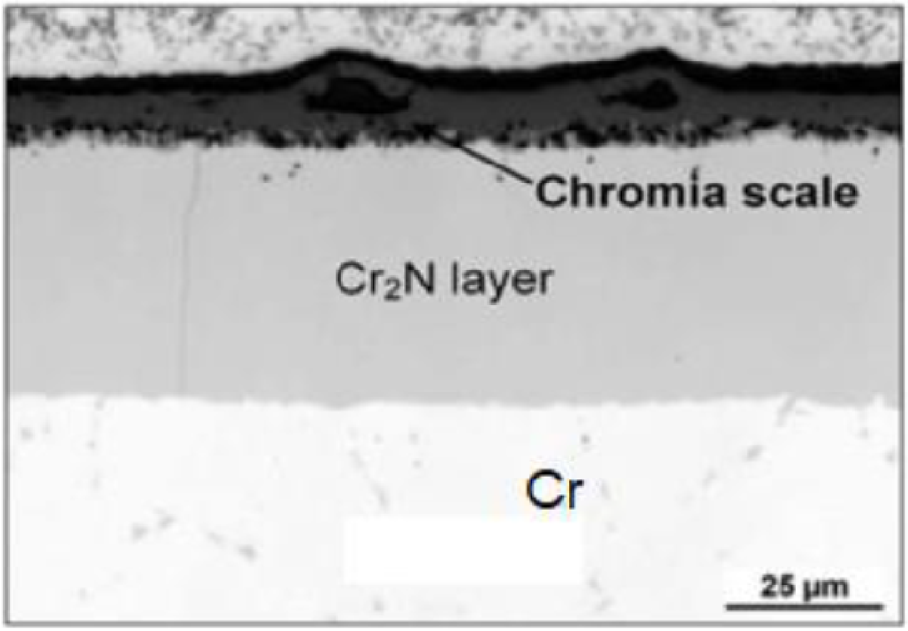

Figure 2.8: Metallographic cross-section after 24 h isothermal oxidation of pure chromium in $N_2 1\% O_2$ at 950°C [19]

resistance[17]. The nitridation effect is found to be high in exhaust gas without water vapour,showing formation of Si_3N_4,resulting in depletion of Silicon.When exposed with water vapor,the nitride formation is found to be lower,showing micro-sized MgSiN_2 at cell boundaries[20].When the conditions are too vulnerable like high temperature,higher ammonia concentration (for example,1%),nickel based alloys could be considered.When increasing the nickel content,it also increases the alloy's nitridation resistance.

2.1.5 Thermodynamic mechanisms

The formation of oxide on the metallic surface will be seen when the potential of oxygen in the environment is much higher than the oxygen partial pressure in the equilibrium with the oxide[21].The oxide will be thermodynamically stable when the standard formation energyΔG° is negative.For example,Cr_2O_3 and Al_2O_3 oxides are stable than other oxide such as NiO because the former have high negative standard free energy of formation.The effective way to predict whether the oxide is likely to be formed is using Elligham's diagram.Fig 2.6 considers oxygen potential and temperature as a two main factors.Example,the Cr_2O_3 oxide at the temperature range of 800°C have the associated equilibrium oxygen partial pressure as 10^{-40} as shown in the figure 2.6.

2.1.6 Environment influence

Oxidation reaction are influenced by many other parallel reactions like nitridation,carburization etc.When considering the case of automotive exhaust system,the exhaust gases influence the oxidation reaction because of its exhaust gas mixture.The exhaust gas mixture contains water,carbon dioxide,sulfur and other particulate matters could change the way of oxidation reaction.The presence of water vapour in the exhaust gas environment could be upto 20% vol and it could cause high oxidation rate in chromium alloyed materials by affecting oxidation response of chromia forming materials;thereby depletion of chromium in the sub-scale region[22].

The presence of carbon dioxide may also affect the oxidation behaviour of the exhaust chromia forming materials.CO_2 and H_2O could cause the transfer of oxygen to the pores in oxide scale and thereby allowing rapid inward passage of oxygen across the pores.And also the surface properties of the material can be affected by initiating carburization or decarburization process.The occurrence of either of the above mentioned processes are based on the carbon activities of both environment and material.In carburizing environments some materials are prone to carburization attack,by aiding the formation of internal carbides that can deplete the material from protective species,for example by the formation of chromium-rich carbides as shown by Kaya et al[23].

Sulfur could be present in the exhaust gas as SO_2 or when reacting with O_2 it can present as SO_3.The sulfur content in the exhaust gas is reduced considerably when comparing to the past because of the strict emission norms for vehicles.However, there is still very less percentage of sulfur present in the synthetic fuel.So,it may affect the oxidation reaction.When comparing to the oxidation rate in pure O_2,the oxidation rate in the atmosphere with SO_2 and O_2 is very rapid because sulfides and oxides are formed parallely[17].

2.2 Materials for High temperature corrosion environments

The engine operating temperature varies according to the type of engine is being used i,e.V6,V8 or V12 have different operating temperatures from the range of 700°C to 1000°C or even more[17].At this temperature,the material might undergo severe thermal cycling,stress and strain,prolonged working time etc,initiates both the surface and mictrostructural changes.The opting material should withstand the thermo-mechanical changes,obtaining high durability and reliability without compromising the cost.The below figure shows the detailed sketch for the different engine types at varied temperatures.

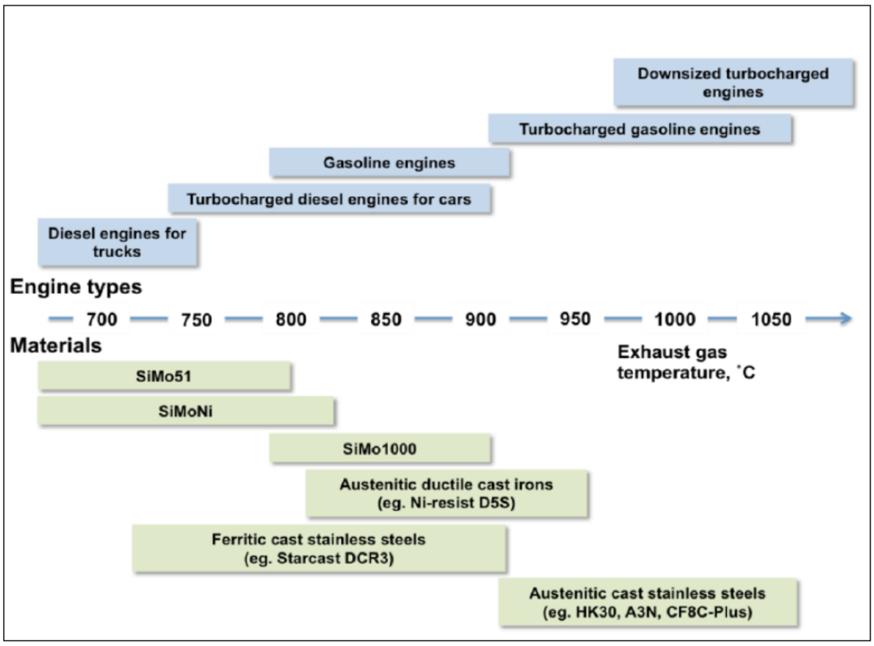

Figure 2.9: Material trends for different engine type at varied temperature[17]

Ferritic cast ductile irons are the most economical choice of material for low temperature applications.The figure 2.9 shows when the temperature is increased the material become more expensive because of its alloying element such as nickel.The commonly used exhaust material is SiMo51 which is a ferritic cast ductile iron with 3% carbon,4% silicon and 0.9% molybdenum content.The operating temperature for this material is at the range of 400-800°C,when operating at higher temperatures further alloying elements like Ni,Al are required.The inclusion of these alloying elements improves mechanical properties and also the corrosion resistance.Nowadays,at higher temperature Ni based materials preferred.In this thesis work,austenitic cast stainless steels-HK30,one of the materials mentioned in the figure 2.9 is used among other candidate materials for the study of their behaviour in highly corrosive environments with higher ammonia content at 700°C.

2.2.1 Wrought materials

Wrought materials comparatively have less carbon than the cast materials and also with high chromium content,so they are studied widely for the high temperature corrosion applications.In this,grain size plays a vital role in corrosion resistance;a smaller grain size leads to a faster formation of the chromia protective layer,due to faster diffusion of chromium and less lateral distance required for the oxide to grow further[25].

2.2.1.1 Ferritic stainless steels

Ferrite is a BCC crystal structure and contains 11% to 30% pf Cr,which is mainly used for the medium corrosion resistance applications.Ferritic steels have low thermal expansion coefficient than austenitic steels due to its BCC structure.The ferritic stainless steels have Mo,Cr,C,Si,Mn as their alloying elements;Cr percentage is very low to form the protective oxide layer.

The carbon and nitrogen solubility in the ferritic phase is less certain at low temperatures.When carbon and nitrogen in excess combines with carbide forming alloying element and forms precipitate as carbides or carbo nitrides [26].And precipitation of chromium carbides on the grain boundaries known as sensitization is deleterious to the corrosion resistance[26].

2.2.1.2 Austenitic stainless steels

Austenitic stainless steels have Ni to stabilise the material in lower temperature.For high temperature applications,high amount of Cr along with 2% Mn and 1% Si.They have very good mechanical properties in higher temperatures like 850°C comparing to ferritic grades.To have the protective layer of chromium oxide Cr_2O_3,Cr content above 22% is needed.The austenitic stainless steels used in this work have a maximum of 16%-27% Cr and 10%-22%.The other alloying elements used are Mn,Si and Al which helps in avoiding the evaporation of Chromia in water atmosphere[27].

2.2.2 Cast irons

It is a group of ferrous alloys containing more than 2wt% carbon.They have low melting point and high fluidity,because of high carbon content gives the alloys a good castability[17].

Graphitic cast irons are formed at the end of solidification process;forming graphite precipitates.It is controlled by low cooling rate,higher number of nucleating sites and alloying of elements such as C,Si,Co and Ni.The three types of cast irons are ductile irons,grey irons and compacted graphite irons which are classified according to their graphite nodule shape.Grey irons contain graphite as flakes and found in area where thermal conductivity is much concerned.In automotive exhaust system,where strength and ductility are highly considered,ductile cast irons with spheroidal graphite are chosen.The nodular graphite shape is achieved by adding Mg to the melt.Compacted graphite iron has graphite shapes intermediate between flake and spheroidal[17].

When cooling rate during solidification is high and the number of nucleating sites is less or possibly the melt is with carbide-stabilizing elements such as Cr and Mo,solidification promotes cementite formation,instead of graphite.But,for exhaust gas,the formed primary carbides are typically of the M6C type,its formation is not dependent on the cooling rate.

For ductile irons and cast steels,carbides improve strength but might cause brittleness if large amount are present.Further alloying with Ni,a complete austenitic material could be formed.Elements for stabilizing the austenitic phase are Mn,Cu and N.The ferritic phase can also be stabilized by alloying it with Cr,Ti,Mo,Si or Al[17].

2.2.2.1 Ferritic cast stainless steels

Ferritic grade of cast stainless steels have considerably less high temperature strength when comparing to austenitic cast stainless steels;but have good thermal fatigue resistance due to high thermal conductivity and less thermal coefficient of expansion[28]. This ferritic grade have low amount of carbon which leads to high melting point and less quality of casting.Due to less amount of carbon,the grain size reduction when austenite to ferrite phase transformation around 750°C,is removed because of ferrite forming directly from the melt[17].Example for this type of material is DCR3 developed by Daido Steel Co;this type of material is not the scope of the work.

2.2.2.2 Austenitic cast stainless steels

Austenitic cast stainless steels are usually used where the working conditions are very demanding;their higher nickel content makes them expensive among other cast stainless steels in market[29].Example of this type of materials is HK30 with 0.25-0.35%C,23-27%Cr,19-22%Ni (Fe,bal) as shown in table 3.1.The high nickel content aids in maintaining the austenite structure in the room temperature.While comparing to other cast irons,HK30 has better mechanical properties at elevated temperatures.However,less carbon content and lack of graphite structure makes it not a good option as castability[29].

3

Methods

3.1 Materials

The 9 candidate materials for this thesis work were provided by Outokumpu according to the European standards as shown in the table 3.1.The table shows the 5 wrought materials and 4 cast materials.

Materials	Phase	C%	Cr%	Mn%	Si%	Ni%	Mo%	N%	Fe%
1.4662	Ferrite	0.010	21	0.39	0.43	0.2		0.016	Bal
1.4509	Ferrite	0.019	17.83	0.33	0.67				Bal
1.4951	Austenite	0.046	25.21	0.85	0.58	19.02	0.16	0.032	Bal
1.4307	Austenite	0.018	18.2	1.52	0.45	8.1		0.056	Bal
1.4404	Austenite	0.016	17.2	1.55	0.60	10.1	2.04	0.046	Bal
713C	Ni base	<0.2	11-14	<1.0	<1.0	Bal	3.5-5.5		
HK30	Austenite	0.405	19.57	1.26	0.97	15.02	<0.01		Bal
SiMo51	Ferrite	3	0.1	0.4	4		0.9		Bal
SiMo51(*)	Ferrite	3	0.1	0.4	4	0.9			Bal

Table 3.1: Alloy chemical composition in wt%

Material	*	Ni%	Cr%	W%	Mo%	Fe%
SiMo51 (*)	coating	Bal	15.5	4.5	16	4

Table 3.2: Coating chemical composition of SiMo51 in wt%

3.1.1 Alloying of Wrought materials

1.4509 is a wrought ferritic stainless steel with body centered cubic structure (bcc) which contains less carbon when compared to cast stainless steels (see.table 3.1), 18% cr content and Fe balance which also have Niobium and Titanium as a stabilizing alloy.The Niobium content provides good oxidation and corrosion resistance when the material is exposed in high temperature gas environments with good strength.The microstructure reveals the ferritic phase with Chromium rich carbides in the grain boundaries.1.4951 is a austenitic stainless steel with face centered cubic (fcc) which have high nickel and chromium content gives a high corrosion resistance property than the ferritic grades.The microstructure show carbides in the grain boundaries and also twinning bands are seen in the microstructure which could increase its strength.Austenitic stainless steels may undergo microstructural changes such as formation of intermetallic precipitation or carbides.

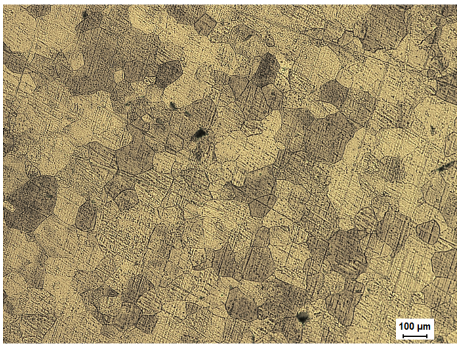

Figure 3.1: Light Optical Microscopy (LOM) image at x100 magnification for 1.4509 ferritic stainless steel electrolytically etched with 10% aqueous oxalic acid with 3A and 10V for 15s.

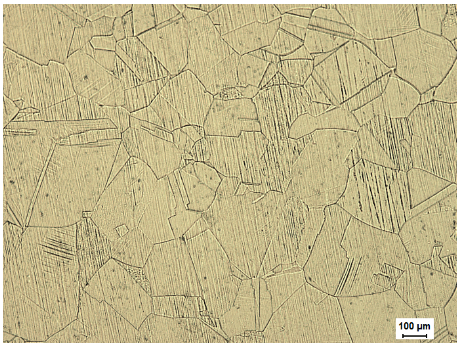

Figure 3.2: Light Optical Microscopy (LOM) image at x100 magnification for 1.4951 austenitic stainless steel Swab etched with Nital 2% for 15s (ASTM E407-07e1).

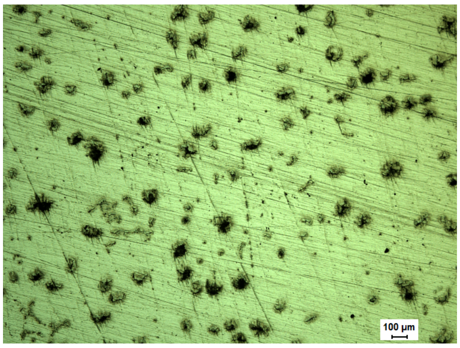

Figure 3.3: Light Optical Microscopy (LOM) image at x100 magnification for SiMo51 ferritic ductile cast iron electrolytically etched with 10% aqueous oxalic acid with 3A and 10V for 15s (ASTM E407-07e1).

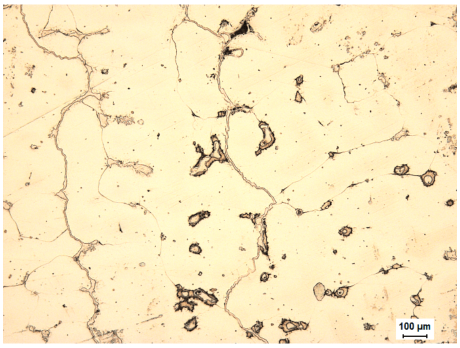

Figure 3.4: Light Optical Microscopy (LOM) image at x100 magnification for HK30 cast austenitic stainless steel swab etched with Nital 2% for 15s (ASTM E407-07e1).

3.1.2 Alloying of Cast materials

SiMo51 is a ferritic ductile cast iron with silicon and molybdenum content which is widely used for exhaust manifold. Silicon provides the higher oxidation resistance by forming the silicon oxide layer on the oxide and metal interface.The microstructure shows the spheroidal graphite nodules in ferritic matrix and these have better oxidation resistance because of the way the nodules is distributed in the ferritic matrix[30].HK30,a cast austenitic stainless steel having good mechanical properties at high temperature when compared to the ferritic materials.This material have high chromium and nickel content which makes it more prone to be corrosion resistance material.The microstructure in figure 3.4 shows the continuous carbides which could affect the mechanical properties and it reveals that it contain more chromium carbides in the matrix.

Figure 3.1 and 3.2 show the microstructure using Light Optical Microscopy

(LOM) of wrought stainless steels before exposure. Figure 3.3 and 3.4 show the microstructure using Light Optical Microscopy (LOM) of cast stainless steels before exposure.

3.1.3 Sample preparation

The materials were cut using water jet cutting machine to obtain the samples of size around 20mm length,15mm width and 6mm height.Samples were grinded in SiC paper until the grit size of P1200 using Struers LabPol-21 on all six edges with reference to the standard ISO 6344-3:1998.The samples were cleaned ultrasonically using ethanol for 10 minutes for each sample and stored in a exicator in order to avoid the formation oxidation products.

The samples were then weighed using the Mettler analytical balance AE240 with the resoltuion of 0.1mg. Then the samples were measured for their length,width and height using the Cockraft vernier caliper with the least count of 0.005mm.Finally,the surface area for all the six sides was calculated.The surface area can be calculated using 3.1,

$$\text{Surface area} \longrightarrow 2\,(\text{hl} + \text{hw} + \text{lw}) \tag{3.1}$$

where, l is the length,h is the height and w is the width. The weight of the alumina (Al_2O_3) crucible were also measured using the same analytical balance for the calculation of gross mass gain of the sample after exposure.

3.1.4 Furnace Calibration

The TMH/12/100/750 three zone horizontal tube furnace is from Elite thermal systems limited.The silica tube is of inner diameter 48mm and heating zone length of 750mm.The furnace is programmed for the desired duration of the exposure of 168hours at two different temperatures such as 550°C and 700°C.This furnace is calibrated using the thermocouple of N-type with diameter of 3mm,length of 1000mm and having the correction factor for 550°C and 700°C according to the standard ASTM E220-07a, ASTM E230/E230M11e1, or ASTM E1350-07.

$$\text{Corrected value} \longrightarrow \text{Obtained value} + \text{Correction factor} \tag{3.2}$$

3.1.5 Exposure

Atmosphere	Gas composition	Temperature (°C)	Duration
Reference	$5\%O_2$+$10\%CO_2$+$10\%H_2$O+N_2	550°C	168h
Exhaust gas	$5\%O_2$+$10\%CO_2$+$10\%H_2$O+N_2+$1\%NH_3$	550°C	168h
Reference	$5\%O_2$+$10\%CO_2$+$10\%H_2$O+N_2	700°C	168h
Exhaust gas	$5\%O_2$+$10\%CO_2$+$10\%H_2$O+N_2+$1\%NH_3$	700°C	168h

Table 3.3: Exposure matrix

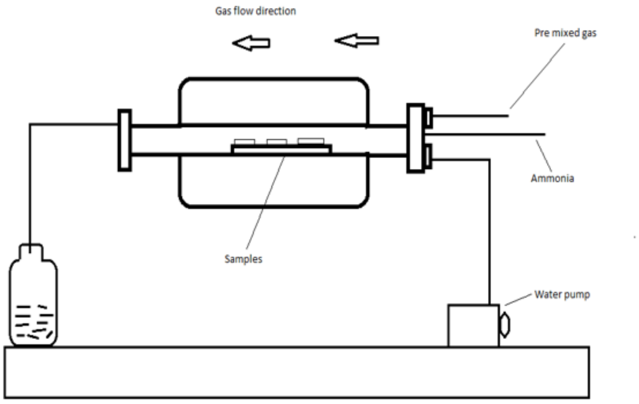

Figure 3.5: Schematic view of the high temperature furnace used

After calibrating the furnace to the required temperature,the gas flow is set. The flow with 5%O_2,10%CO_2,10%H_2O and remaining percentage is N_2 set for the reference exposures at temperatures of 550°C and 700°C. The main exposure includes 5%O_2,10%CO_2,10%H_2O,N_2 and 1% of NH_3.The total flow of the gas is pre-set to be 250mL/min at room temperature.Samples are kept in the alumina crucible (Al_2O_3) as shown in the figure 3.6 below and placed in the calibrated temperature zone at the furnace tube as shown in the figure 3.5,then the system is closed and tightened to avoid the gas leakage.

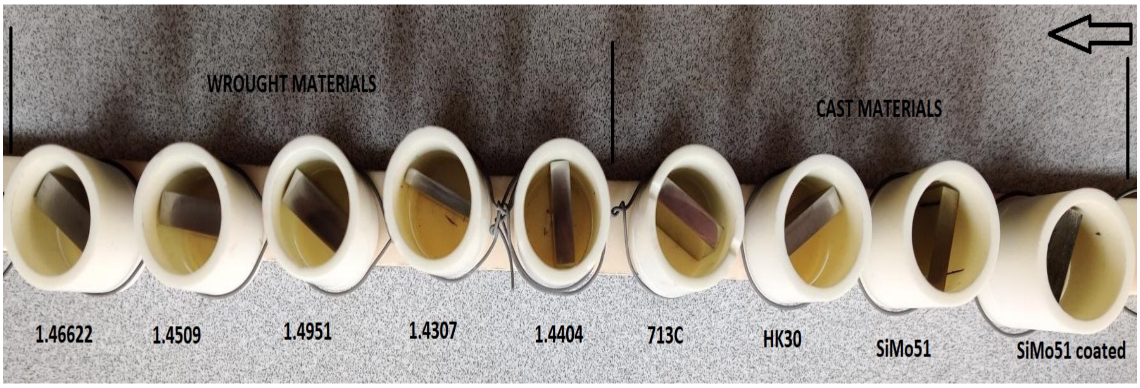

Figure 3.6: Samples in the Alumina crucible

Now the program is switched ON to reach the desired temperature.The Argon (Ar) gas is used to remove the other gases from previous exposure and also to ensure that the system is tightly closed and the temperature is allowed to reach the required point and atmosphere is switched ON.The overall exposure is based on the standard ISO 21608:2012(E).

3.1.6 Mass calculations

The mass calculations are related to the oxide layer thickness to determine the oxide kinetics.There are two mass changes such as gross and net were recorded.The gross mass change is the measure of the spalled oxides in the crucible.It was measured by dividing the equation 3.3 by surface area,

$$\Delta \mathrm{m_g} \longrightarrow \mathrm{m_{SC}(t) - m_{SC}(t_0)} \tag{3.3}$$

where $m_g(t)$ is the gross mass change at the time (t_n),
$m_{SC}(t)$ is the mass of the crucible and the test piece,
$m_{SC}(t_0)$ is the mass change of tHe crucible and the test piece before the test.

The net mass change is obtained from dividing the equation 3.4 by the surface area calculated.

$$\Delta \mathrm{m_{net}} \longrightarrow \mathrm{m_S(t) - m_S(t_0)} \tag{3.4}$$

where mNET is the net mass change in time t, mS is the mass of sample at time t, mS (t0) is the mass os sample prior to the test.Finally, the gross mass gain and net mass gain were plotted together to find the mass gain for each material.The mass calculations were performed according to the standard ISO 21608:2012(E).

3.1.7 Light Optical Microscopy (LOM)

The Zeiss optical microscopy was used to view the samples through the magnification lens by the visible light source.LOM was used to get the microstructure of the samples as shown in the figure 3.1-3.4. to show the difference between ferritic and austenitic phases.

3.1.8 Scanning Electron Microscopy (SEM/EDS)

Scanning Electron Microscopy with secondary electrons and back scattered electrons from Zeiss were used in this thesis work to characterize the surface morphology of the materials.SEM allows to scan the focused high energy electron beam on the surface.Electrons were produced from top by the electron gun and travel to the bottom by passing through the lenses and apertures to produce the focused electron beam to hit the sample.The sample were mounted on the sample chamber.The electron beam position on the samples surface was controlled by scan coils above the objective lens.The beam,either rastering or scanning gives the information of the defined area in the sample which has to be collected.With the result of the electron-sample interaction,signals were produced. SEM includes components such as

- electron gun
- electron detector
- column where the electrons travel (first and second condenser lenses
- sample chamber
- computer to display the images,

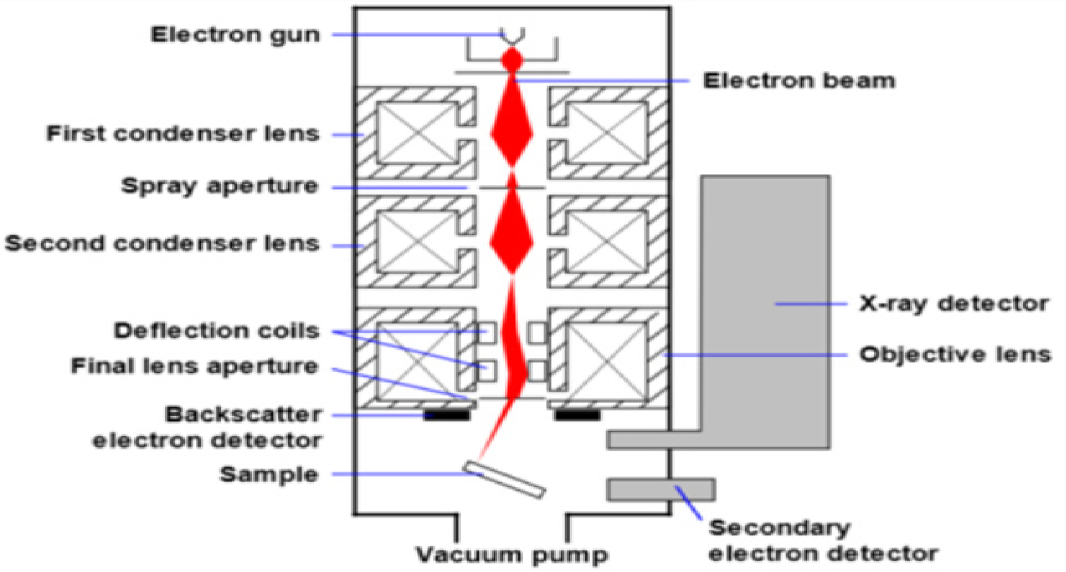

Figure 3.7: Schematic view of the Scanning Electron Microscopy, source - nanoscience instruments.

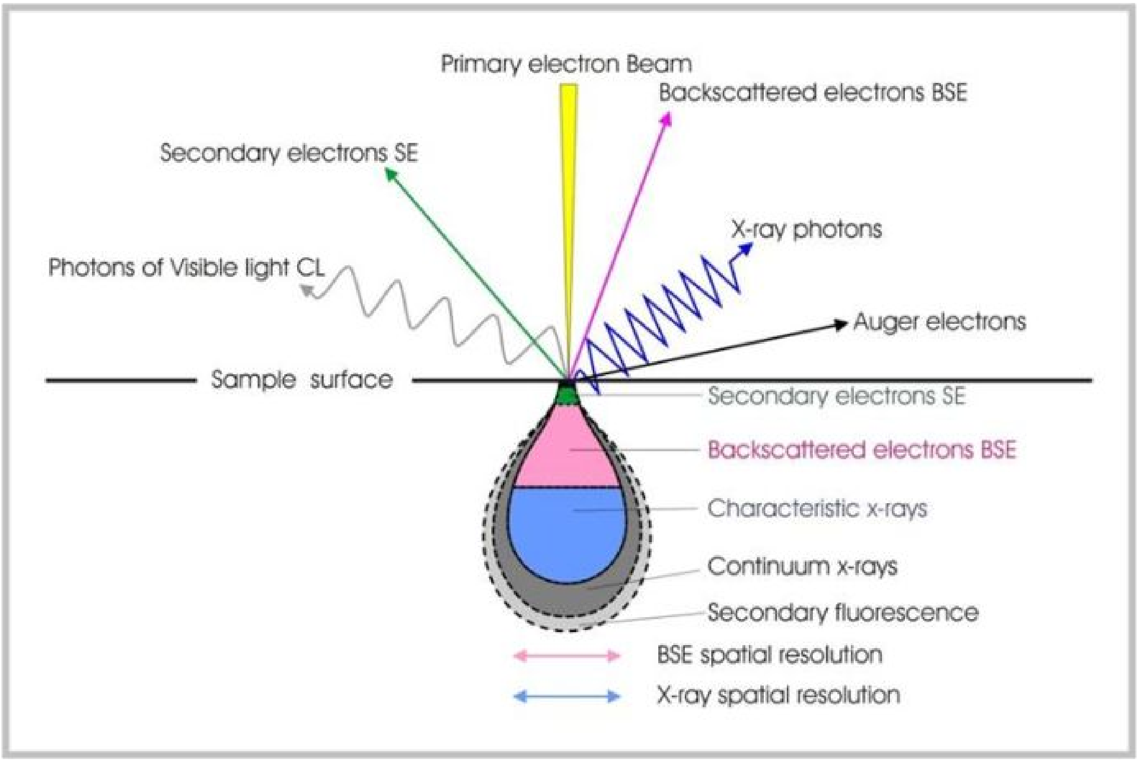

Figure 3.8: Illustration of the difference between back scattered electrons and secondary electrons [31].

as shown in the figure 3.7.

The produced signals such as back scattered electrons and secondary electrons were used to obtain information about the surface morphology and composition of the material examining.When electron beam hit the sample it penetrated for few microns depending on the accelerating voltage and density of the sample.Many signals like secondary electrons and back scattered electrons were produced during the interaction with the sample. The resolution of SEM depends on the factors such as electron spot size, interaction volume of the beam etc.[32].Figure 3.8 shows the difference between secondary electrons and back scattered electrons.The secondary electrons were emitted by atoms near the surface or a near surface of a material when the electrons became excited and had sufficient energy to escape the surface.Secondary electron imaging was more surface sensitive and had greater resolution.By losing energy while exciting the electrons within the sample,electrons from the incident beam also undergo backscattering and they re-emerge from the surface.Escape depth of backscattered electrons can be greater than that of the former,surface morphological characteristics can be affected.However the latter electrons, have the advantage of being sensitive to the atomic mass of the nuclei from which they scatter. As a result, heavier elements which were back-scattered more efficiently, appeared brighter than the lighter elements in a backscattered electron image[33].

The difference between the secondary electrons and back scattered electrons is shown in the figure 3.9 and 3.10 respectively.The BSE in figure shows brighter view of nickel comparing to other elements present in the surface such as Cr,F,Mn; due to the large number of detected back scattered electrons which is proportional to atomic number (Z,nickel-28) comparing to other elements present.With the help of BSE,it was possible to get an overview of surface composition as well.

The secondary electron image in the figure 3.9 show the better topographic view of the exposed samples like defect holes in Ni.The SE detectors has low energy comparing to BSE detectors.

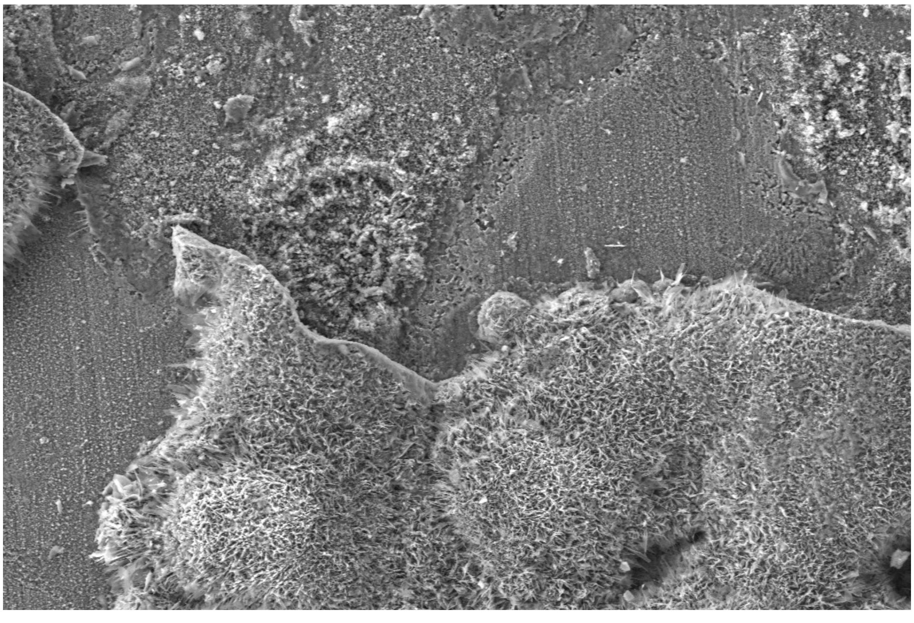

Figure 3.9: SEM image of HK30 from exhaust gas environment with 1% of NH_3 in 700°C,viewed at 1.01K magnification in secondary electron detector.

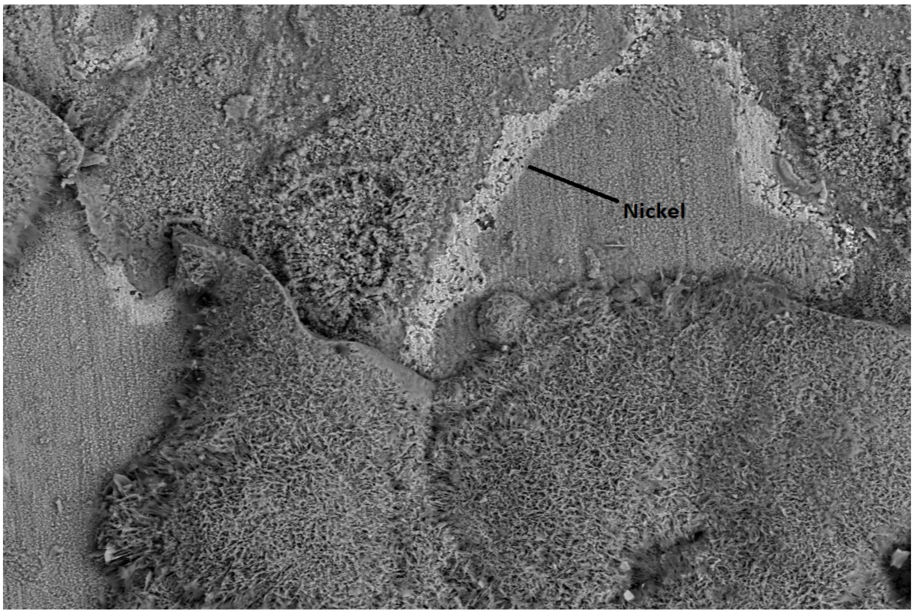

Figure 3.10: SEM image of HK30 from exhaust gas environment with 1% of NH_3 in 700°C,viewed at 1.01K magnification in back-scattered electron detector.

3.1.9 X-ray Diffraction (XRD)

X-ray diffraction (XRD) was used to find the phase of the crysralline material.XRD is a powerful nondestructive technique used for characterizing crystalline materials and materials like fluid,polymers,thin film coatings etc. It gives information about the structures,phases,crystal orientation,structural parameters such as average grain size,the existence of the defects in a crystal,degree of crystallinity etc.X-ray diffraction peaks were produced by constructive interference of a monochromatic beam of X-rays scattered in particular angles from each set of lattice planes on a sample.The intensity of the peaks were determined by the distribution of atoms within the lattice[34].The X-rays were generated by the cathode ray tube which were filtered to produce monochromatic radiation then concentrated by collimation and rays hit the sample at an angle of θ as shown in figure 3.11.

The interaction of the incident rays on with the sample gives out the constructive interference when it obeys Braggs law shown in equation 3.5.

$$\mathrm{n}\lambda \longrightarrow 2\,\mathrm{dsin}\theta \tag{3.5}$$

where n is integer,λ is the wavelength,d is the interplanar spacing and θ is the diffraction angle.Figure 3.12 explains the basic principle of Bragg's law.Braggs law gives the relaiton between the wavelength of the electromagnetic radiation to the diffraction angle and the lattice spacing in crystalline material.

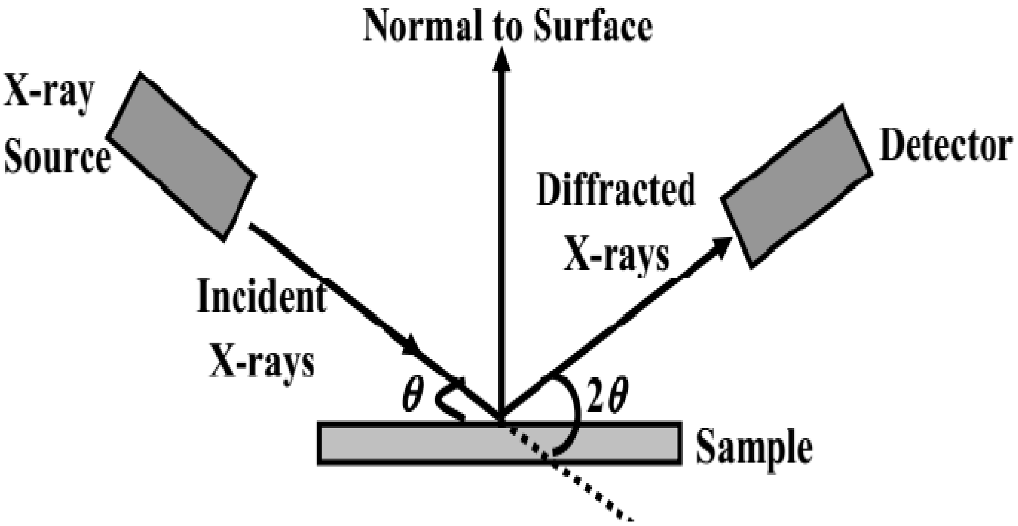

Figure 3.11: Schematic view of the working principle of X-ray Diffraction[35].

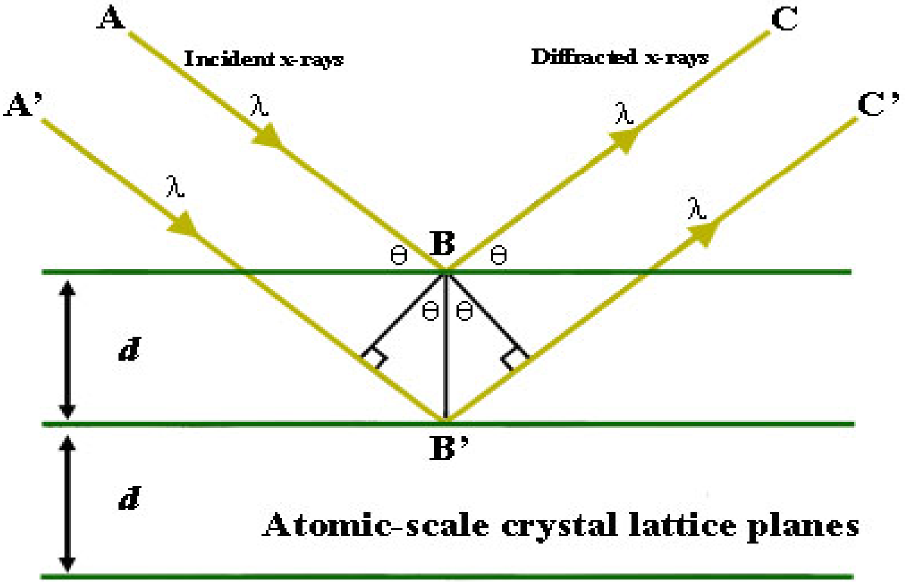

Figure 3.12: Principle of Bragg's law [36].

3.1.10 Glow-discharge optical emission spectroscopy (GD-OES)

GD-OES is used qualitative and quantitative analysis method for ferrous and non-ferrous materials.It is a measure of depth profile of elements in a sample with the help of detecting emissions containing atoms with plasma through sputtering.The measuring ability is <50nm to many hundreds of μ.

It was filled with Argon gas at low pressure of (0.5 – 10 hPa). Direct voltage (DC) was applied between the anode and the sample.The DC voltage made electrons to be released from the surface of sample and was driven toward the anode acquiring more kinetic energy.The electrons transferred their kinetic energy to Argon atoms

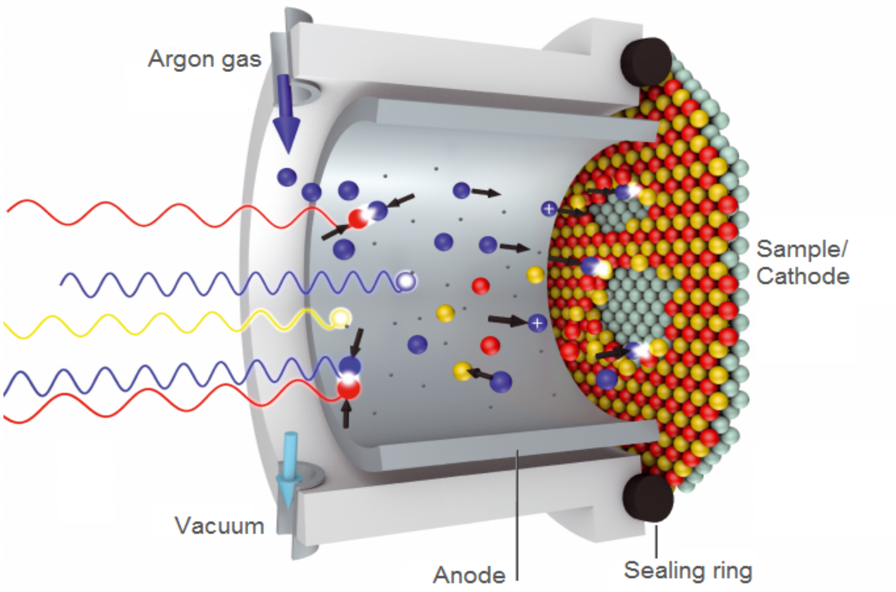

Figure 3.13: Principle of GD-OES [37].

due to inelastic collision,which dissociated as Argon cations and electrons.This type of avalanche effect triggered an rise in density of a charge carrier making Argon gas as conductive.Eventually,the mix of neutral Argon atoms and free charge carriers (which was Argon cations and electrons) is known as plasma.

The Argon cations were driven to the sample surface because there was huge negative potential.While striking the sample surface the Argon cations knocked out of sample atoms.This process is called as sputtering.

The high-energy electrons then collided with removed atoms from the sample.While these collisions,energy was transmitted to the sample atoms aiding them to reach excited states.Then the atoms emitted light with a characteristic wavelength spectrum when returning to ground state.

During their passage through the entrance slit,emitted light reached the concave grating where it was dispersed as spectral components.These spectral components were recorded by the detection area.The obtained intensity of the lines are equal to the intensity of the corresponding element within the plasma[37].

4

Results

After exposing all the candidate materials in the simulated exhaust gas environment with and without ammonia in two different temperatures of 550°C and 700°C,samples showed thin and thick oxide scale growth,severe spallation was observed in materials like SiMo51,1.4307.Let us see the observations from all 9 candidate materials in this section.

4.1 Exposed samples

The samples exposed at 550°C for 168h are shown below.The samples from 550°C formed very thin oxide layer on the surface and comparatively less spallation than 700°C can be seen.Since,samples exposed in 550°C has thin oxide layer,it can be assumed that the oxidation rate could have been slow.

(a) 1.4622-reference **(b)** 1.4622-1%NH_3

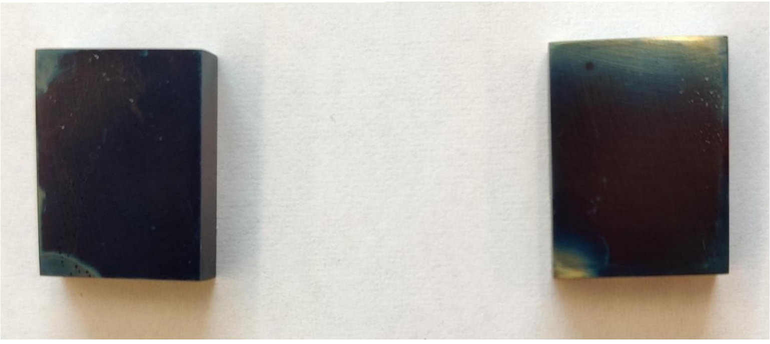

(c) 1.4509-reference **(d)** 1.4509-1%NH_3

Figure 4.1: Images of the exposed samples 1.4622 and 1.4509 at 550°C for 168h

(a) 1.4951-reference **(b)** 1.4951-1%NH_3

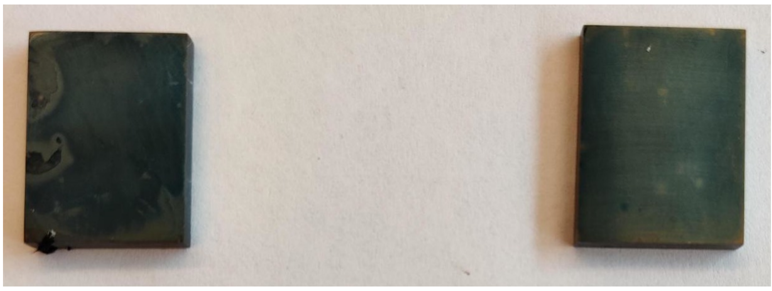

(c) 1.4307-reference **(d)** 1.4307-1%NH_3

Figure 4.2: Images of the exposed samples 1.4951 and 1.4307 at 550°C for 168h

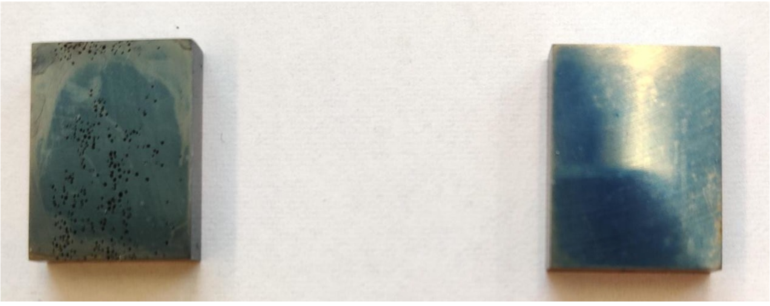

(a) 1.4404-reference **(b)** 1.4404-1%NH_3

Figure 4.3: Images of the exposed samples 1.4404 at 550°C for 168h

(a) SiMo51-reference **(b)** SiMo51-1%NH_3

(c) HK30-reference **(d)** HK30-1%NH_3

Figure 4.4: Images of the exposed samples SiMo51 and HK30 at 550°C for 168h

(a) SiMo51 coated-reference **(b)** SiMo51 coated-1%NH_3

(c) 713C-reference **(d)** 713C-1%NH_3

Figure 4.5: Images of the exposed samples SiMo51 and HK30 at 550°C for 168h

The samples exposed at 700°C for 168h are shown below.The samples from 700°C formed thick oxide on the surface and showed more spallation than 550°C.The possible nitridation temperature is from 250°C to 700°C[2].Since it has thick oxide layer,there could be rapid oxidation.

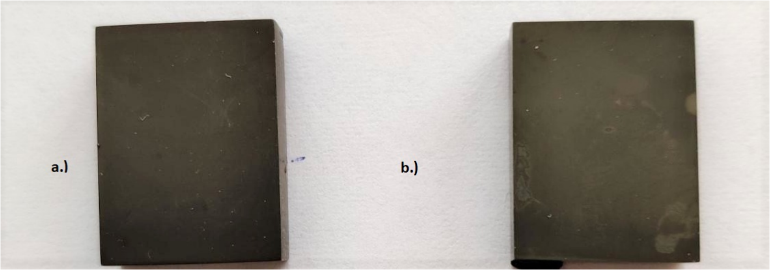

(a) 1.4622-reference **(b)** 1.4622-1%NH_3

(c) 1.4509-reference **(d)** 1.4509-1%NH_3

Figure 4.6: Images of the exposed samples 1.4622 and 1.4509 at 700°C for 168h

(a) 1.4951-reference **(b)** 1.4951-1%NH_3

(c) 1.4307-reference **(d)** 1.4307-1%NH_3

Figure 4.7: Images of the exposed samples 1.4951 and 1.4307 at 700°C for 168h

(a) 1.4404-reference **(b)** 1.4404-1%NH_3

Figure 4.8: Images of the exposed samples 1.4404 at 700°C for 168h

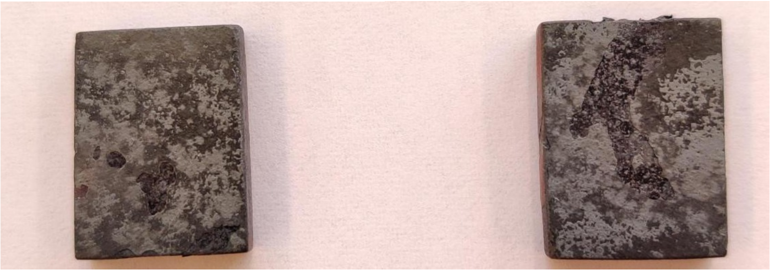

(a) SiMo51-reference **(b)** SiMo51-1%NH_3

(c) HK30-reference **(d)** HK30-1%NH_3

Figure 4.9: Images of the exposed samples SiMo51 and HK30 at 700°C for 168h

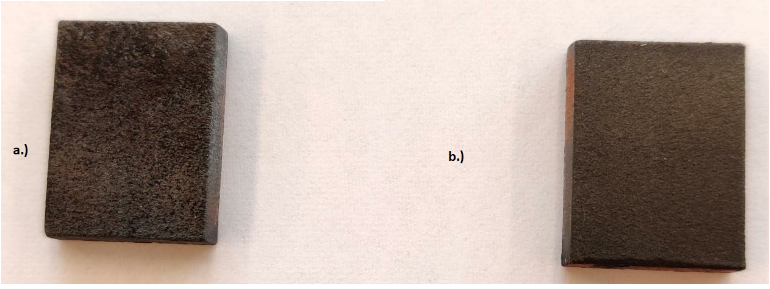

(a) SiMo51 coated-reference **(b)** SiMo51 coated-1%NH_3

(c) 713C-reference **(d)** 713C-1%NH_3

Figure 4.10: Images of the exposed samples SiMo51 coated and 713C at 700°C for 168h

4.1.1 Mass gain

The net mass gain and gross mass gain for reference and 1%NH_3 isothermal exposure at 550°C were plotted.

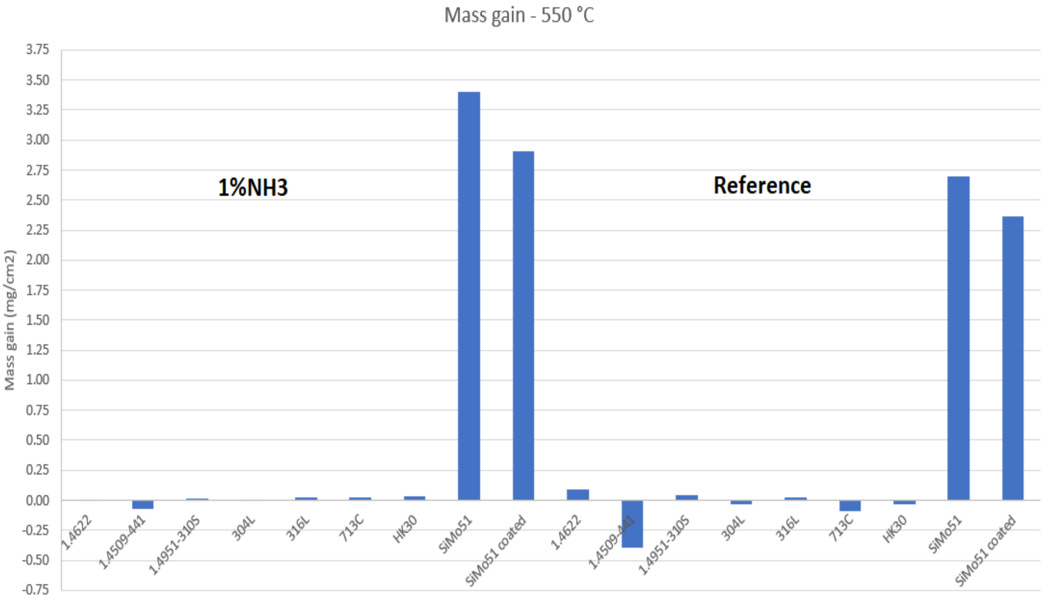

Figure 4.11: Net mass gain of exposure with 1%NH_3 and reference exposure at 550°C for 168h.

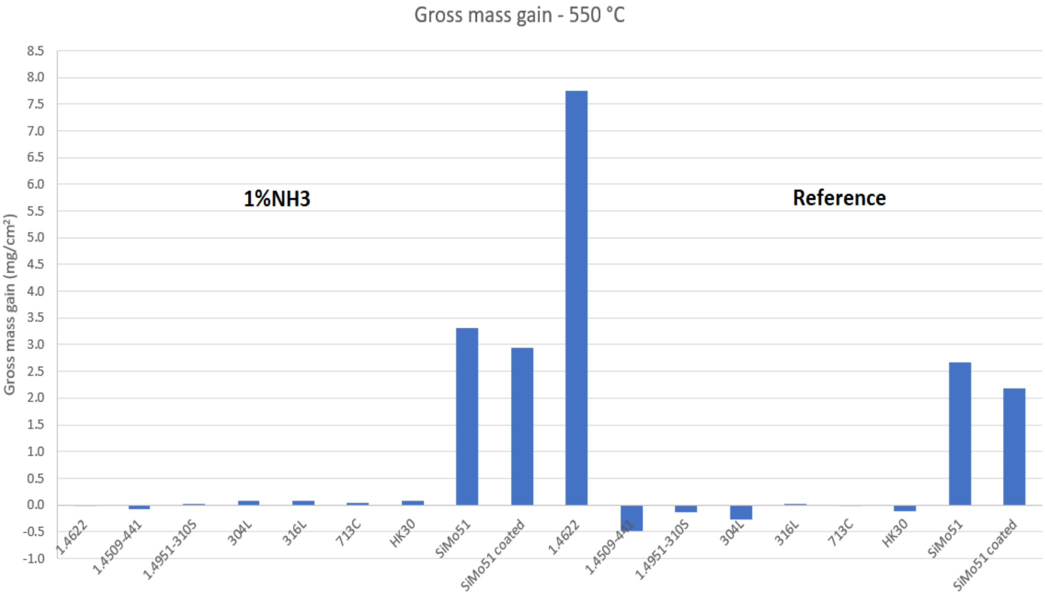

Figure 4.12: Gross mass gain of exposure with 1%NH_3 and reference exposure at 550°C for 168h.

The net mass gain and gross mass gain showed that cast materials like SiMo51 and SiMo51 coated had no oxidation products observed in the crucible (no spallation).Mostly other candidate materials was observed to be with very less spallation or no spallation.

The net mass gain of the SiMo51 increased from 2.69 to 3.40 (mg/cm^2) and SiMo51 coated increased from 2.37 to 2.91 (ma/cm^2).For more detailed investigation regarding the nitrogen uptake in these materials and about the oxide layer thickness; microstuctural characterization was done.1.4509,a ferritic wrought steel showed net mass loss decreased considerably in NH_3 than the reference exposure.The net mass loss changed form -0.39 to -0.08 (mg/cm^2) meaning that it formed the protective thin oxide layer on its surface in N_2 rich atmosphere.All other materials such as HK30,1.4951,1.4307 and 1.4404 showed decreased mass loss or positive net mass gain.The protective species in this thin oxide layer will be studied further in the SEM/EDX analysis.

4.2 Scanning Electron Microscopy (SEM/EDX)

This section deals with the microstructural characterization of the candidate material's,surface morphology and composition and oxide layer.The choice of material for cross section was confined to four candidate materials such as 1.4509,1.4307,SiMo51 and HK30 in order to explain more detailed behavior of material grades like ferritic and austenitic of both wrought and cast material groups.Another important reason for the selection of material for cross section is that these are currently used by SCANIA CV AB in exhaust system of heavy duty trucks.

4.2.1 1.4622

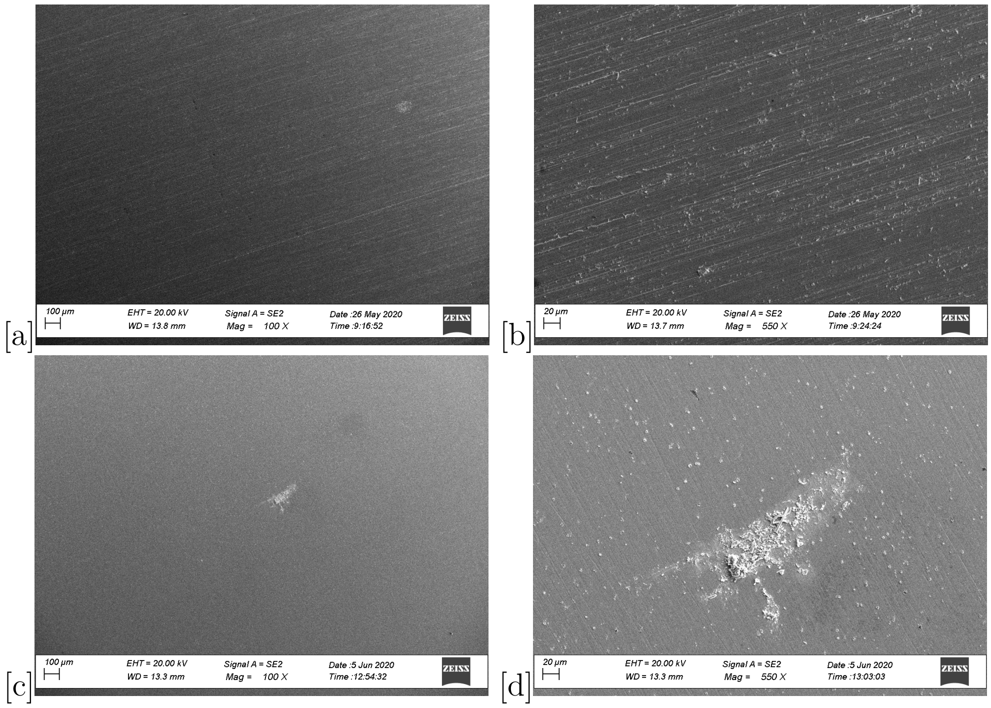

Figure 4.13: a and b are SEM plane view of 1.4622 exposed without ammonia at 550°C for 168h (100x and 550x) using secondary electron detector,c and d are SEM plane view of 1.4622 exposed with ammonia at 550°C for 168h (100x and 550x) using secondary electron detector.

1.4622,a ferritic wrought material developed thin oxide scale when exposed at 550°C shown in fig 4.13.The grinding marks add further confirmation that it is thin oxide scale.The oxide scale is with mixed iron oxide (considerable amount of Mn,Ni,Zn,Nb,Si) in it.The presence of Nb and Cu in sample exposed at ammonia atmosphere depicts that the matrix is not much effected by the atmosphere.

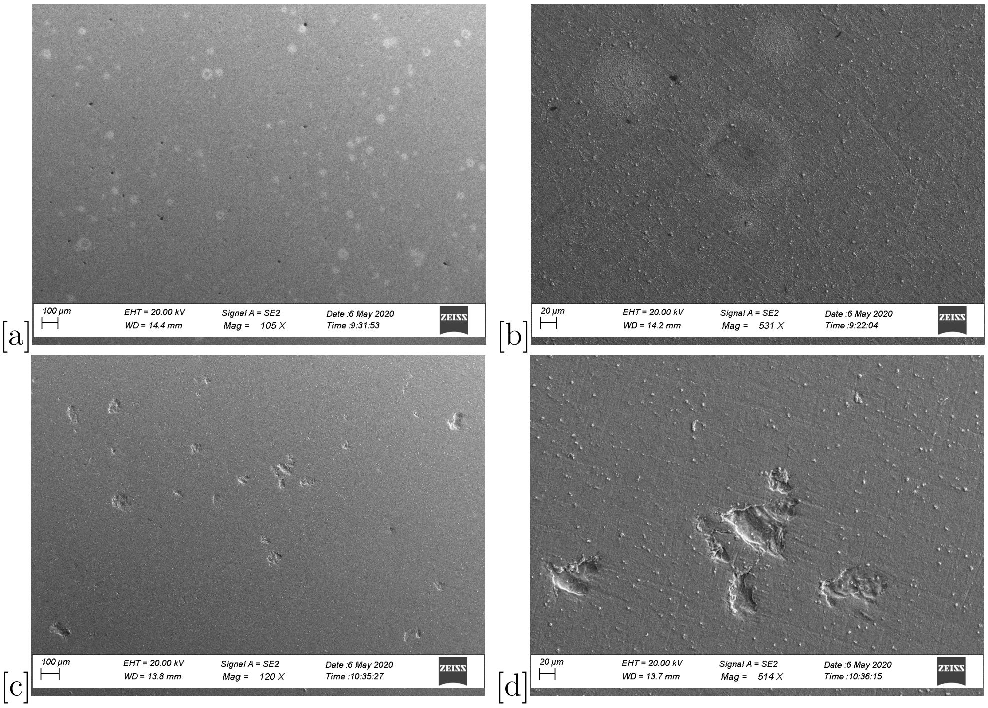

Figure 4.14: a and b are SEM plane view of 1.4622 exposed without ammonia at 700°C for 168h (100x and 550x) using secondary electron detector,c and d are SEM plane view of 1.4622 exposed with ammonia at 700°C for 168h (100x and 550x) using secondary electron detector.

4.2.2 1.4509

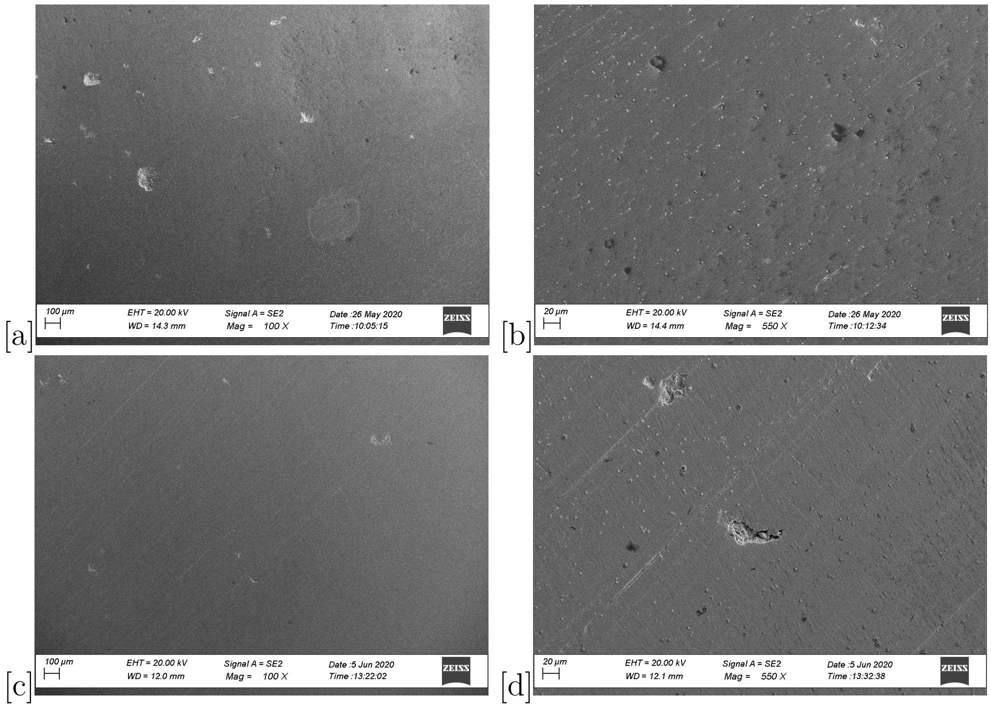

Figure 4.15: a and b are SEM plane view of 1.4509 exposed without ammonia at 550°C for 168h (100x and 550x) using SE detector,c and d are SEM plane view of 1.4509 exposed with ammonia at 550°C for 168h (100x and 550x) SE detector.

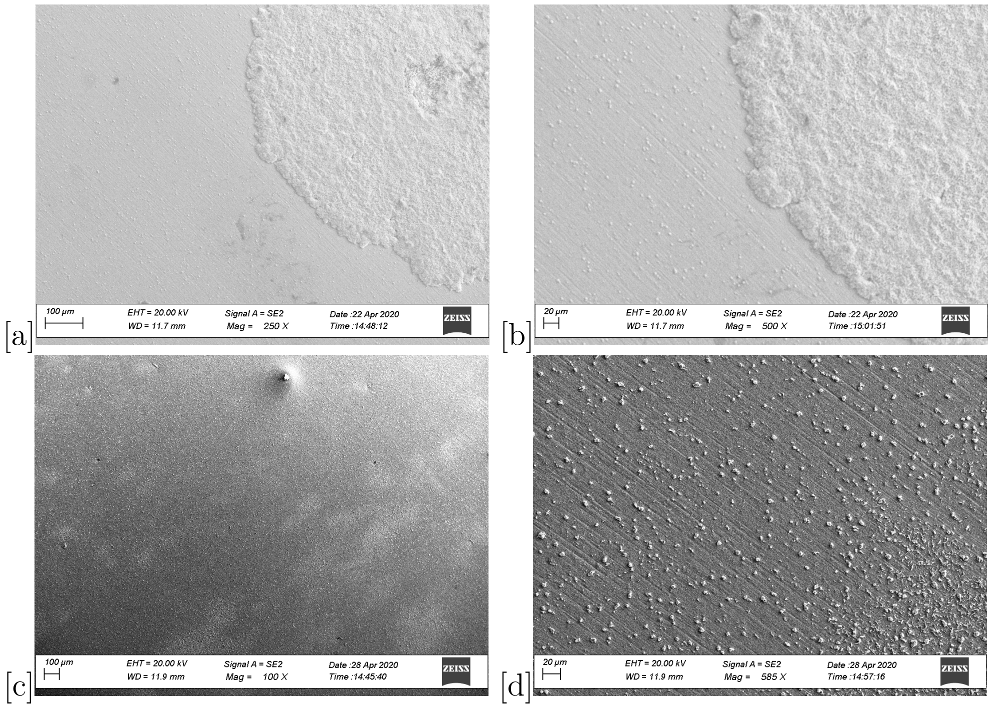

Figure 4.16: a and b are SEM plane view of 1.4509 exposed without ammonia at 700°C for 168h (100x and 550x) using SE detector,c and d are SEM plane view of 1.4509 exposed with ammonia at 700°C for 168h (100x and 550x.) using SE detector.

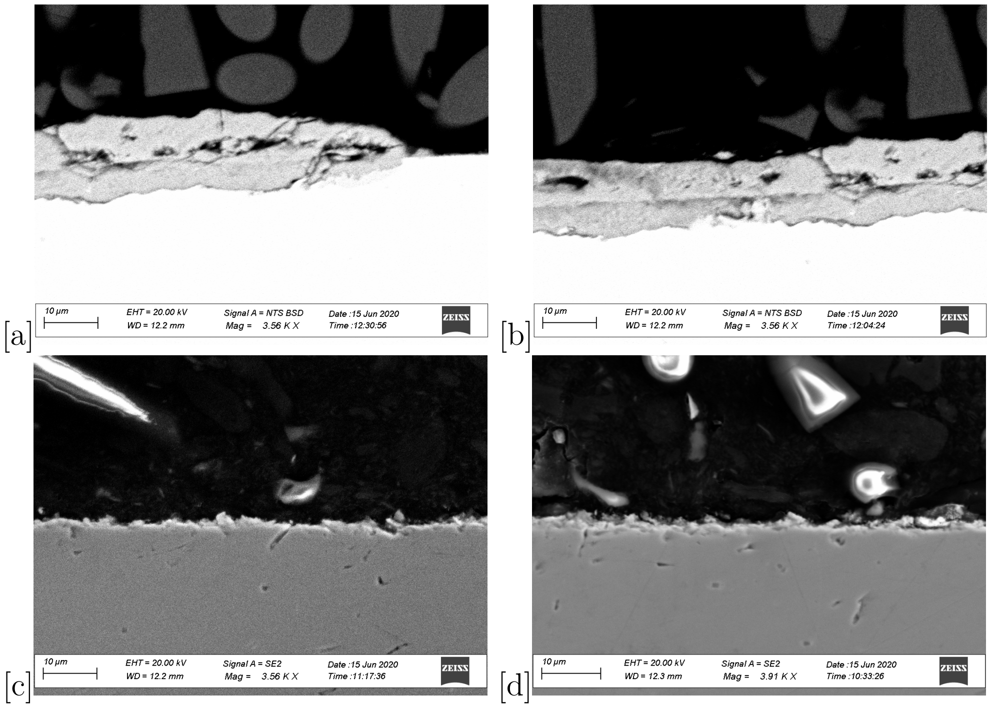

Figure 4.17: (a and b are cross section view of 1.4509 exposed without ammonia at 700°C for 168h (x3.56K) using BSD,c and d are cross section view of 1.4509 exposed with ammonia at 700°C for 168h (x3.56K) using BSD.

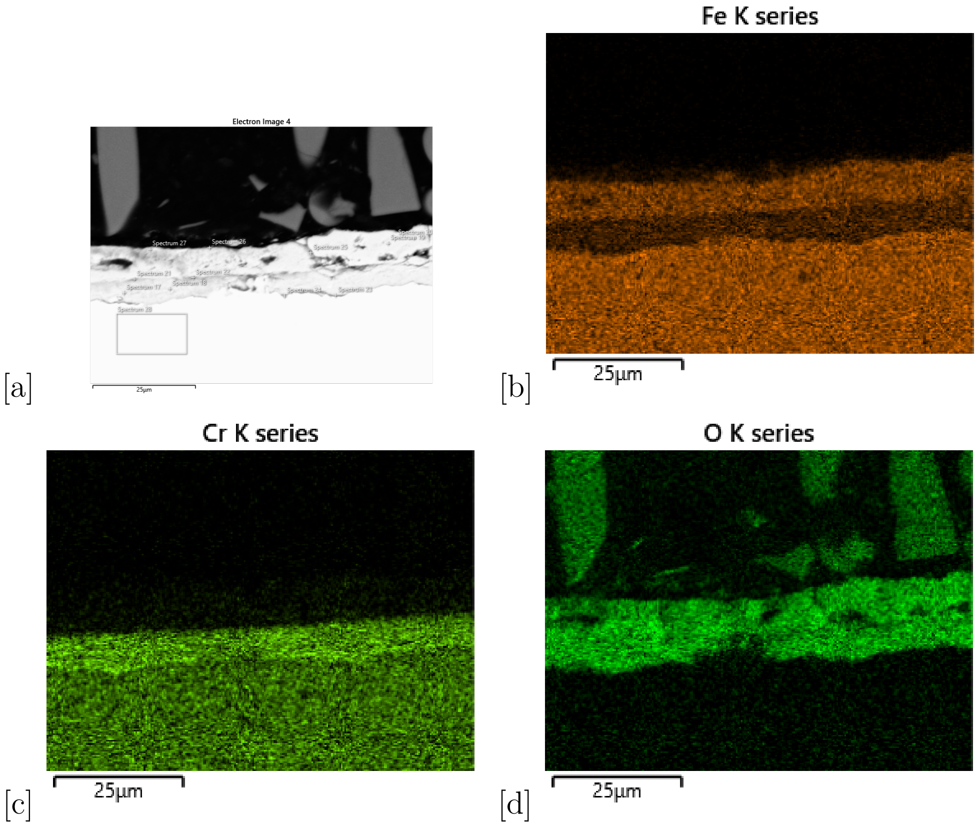

Figure 4.18: Elemental mapping of cross section of 1.4509 exposed without ammonia at 700°C for 168h

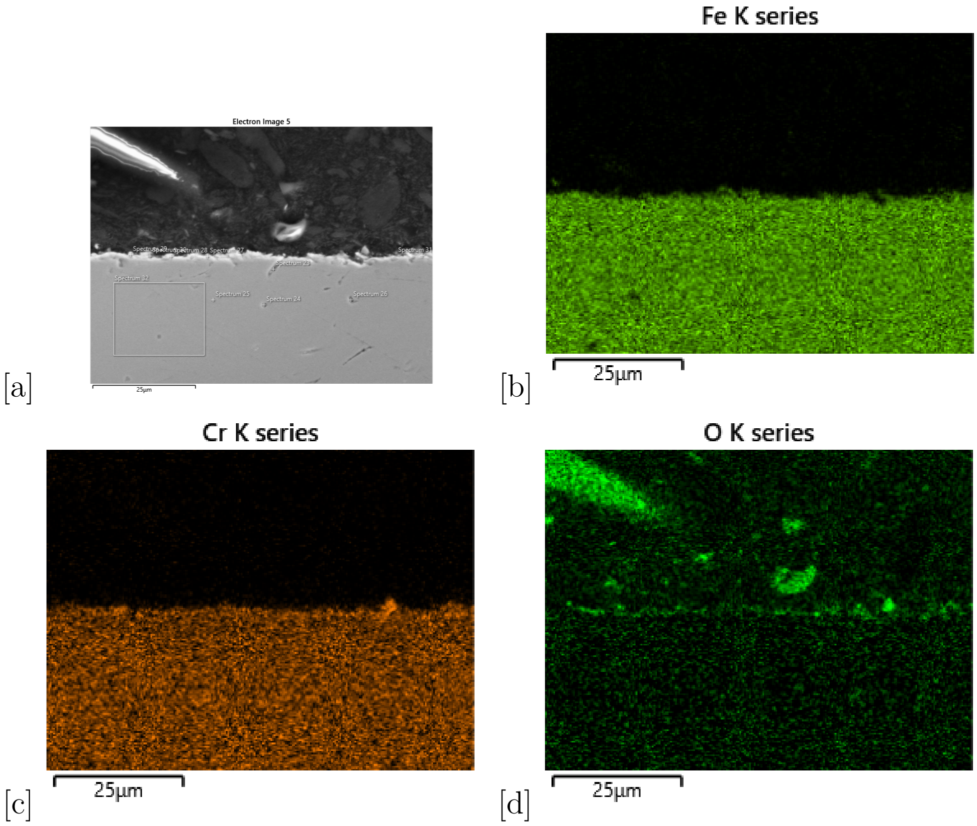

Figure 4.19: Elemental mapping of cross section of 1.4509 exposed with ammonia at 700°C for 168h

This ferritic wrought stainless steel with 18% Cr and very less inclusions of Niobium and titanium exposed isothermally,showed uneven oxide layer in no-ammonia atmosphere and ammonia atmosphere at 700°C.The oxide layers were found to be discontinuous which may be resulted due to the thickness and stress developed with the temperature and atmosphere.The composition of outward oxidation was mostly with Iron oxide and the inward oxidation showed considerable traces of Iron oxide in the Chromium rich oxide layer which makes us to think it might not be the protective oxide layer growing towards the matrix.The morphology showed iron oxides were thick islands distributed unevenly all over the surface of the sample. But,the EDX analysis of reference exposure at 700°C showed the traces of Chromium and Nitrogen below the inner chromium oxide layer.This makes us to assume that the nitrogen diffusion might have occurred through the chromium rich oxide layer.This sample isothermally exposed in ammonia developed a protective Chromium oxide layer despite being discontinuous on the surface.The composition also included considerable amount Si and Mn as well.The thermal stresses because of high temperature resulted in spallation of outermost iron oxide layer in both the atmospheres.

When 1.4509 exposed in 550°C,the grinding marks are still visible so we could say that,it developed a thin oxide layer was thin with no spallation.This might be because of the oxidation process is slow and less thermal stresses acting on the oxide layer.At 550°C,the behavior was like 700°C in some ways like the composition of the outermost layer and inner layer.The Si was detected in the outermost layer along with Chromium oxide.The net mass was decreased in ammonia atmosphere when comparing to non-ammonia atmosphere this could make us think the protective continuous layer was formed.The temperature 550°C showed reasonable behavior with forming protective oxide layer without spallation.With further analysis on the sample like mass calculation on 700°C could be done to conclude the oxide scale formation of 1.4509.

4.2.3 1.4951

1.4951 in fig.4.20,a wrought austenitic material with highest amount of Cr among other materials showed thin oxide scale formation and Cr depletion on the surface of sample without exposed without ammonia;which means percentage of Cr is reduced drastically in some places where Fe is enriched at 550°C.At the same time at 550°C with ammonia,sample showed no drop in Cr percentage on the surface along with Ni,Si,Mn.

For 700°C (fig 4.21),the sample behaved in a different way by developing thick oxide scale which resulted in spallation.In reference atmosphere,formation of mixed thick oxide of Cr and Fe in few places which is assumed to be the outer layer and the inner layer with the same elemental composition additionally with Si content;which could be SiO_2.With ammonia exposure,developed irregular and homogeneous outer layer with Fe oxide and inner layer containing Cr oxide with very little percent of Si and Ni.While accounting spallation,this material had very less spallation comparing to other materials.

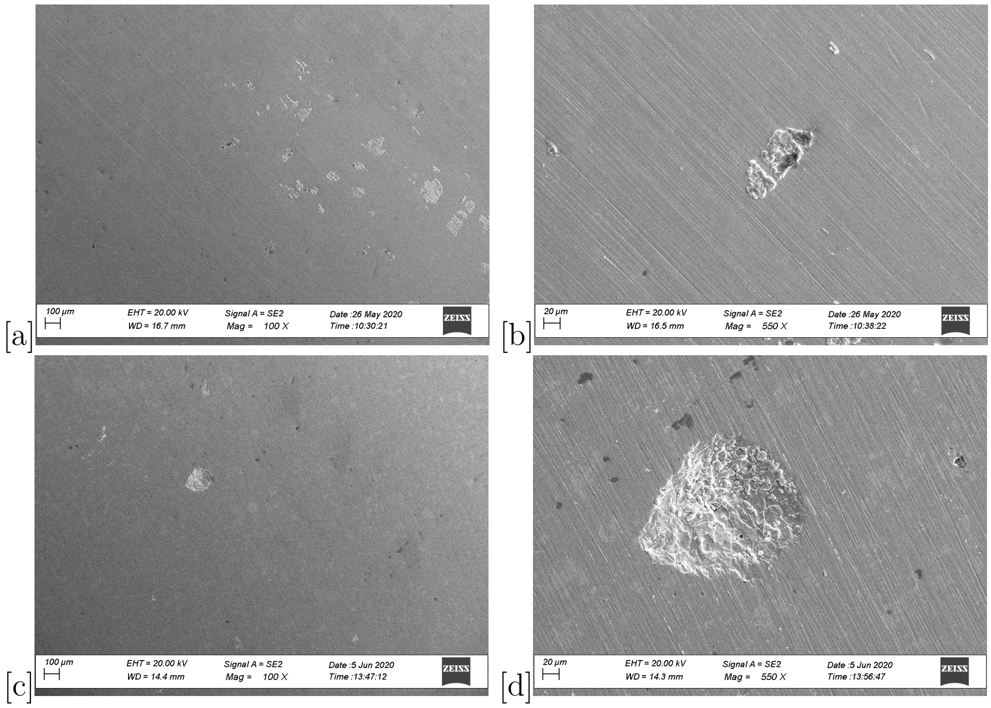

Figure 4.20: a and b are SEM plane view of 1.4951 exposed without ammonia at 550°C for 168h (100x and 550x) using SE detector,c and d are SEM plane view of 1.4951 exposed with ammonia at 550°C for 168h (100x and 550x) using SE detector.

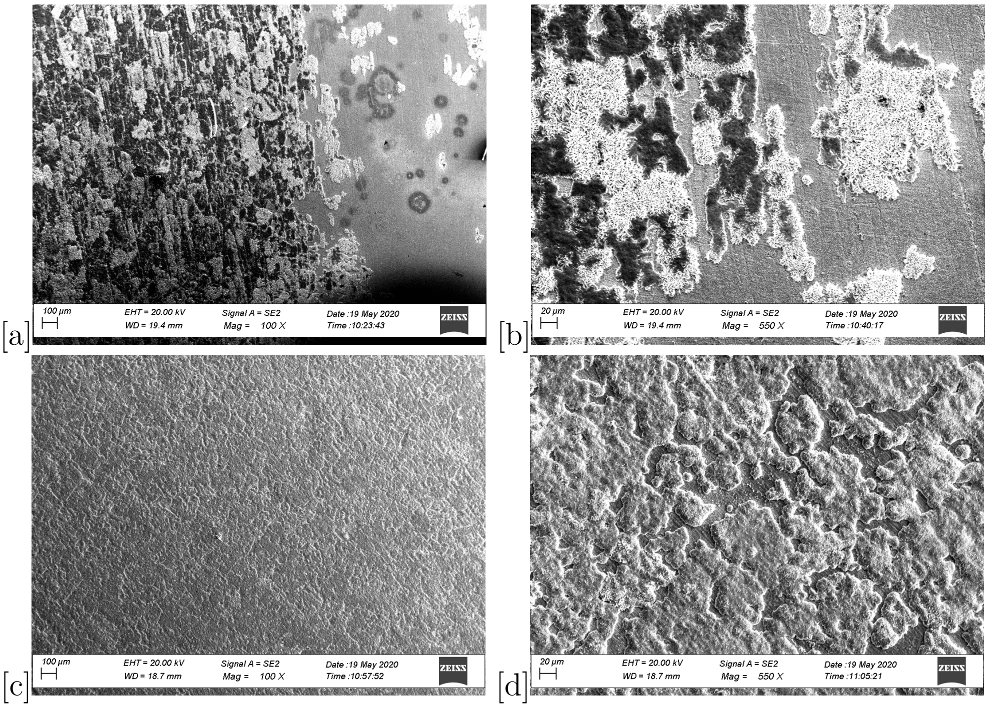

Figure 4.21: a and b are SEM plane view of 1.4951 exposed without ammonia at 700°C for 168h (100x and 550x) using SE detector,c and d are SEM plane view of 1.4951 exposed with ammonia at 700°C for 168h (100x and 550x) using SE detector.

4.2.4 1.4307

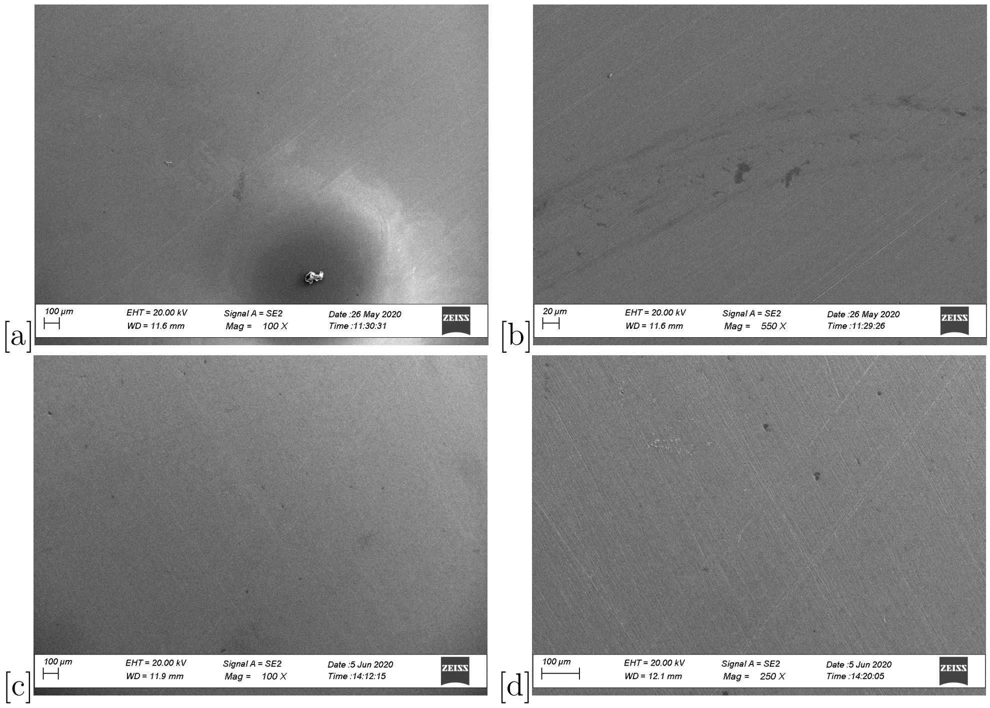

Figure 4.22: a and b are SEM plane view of 1.4307 exposed without ammonia at 550°C for 168h (100x and 550x) using SE detector,c and d are SEM plane view of 1.4307 exposed with ammonia at 550°C for 168h (100x and 250x) using SE detector.

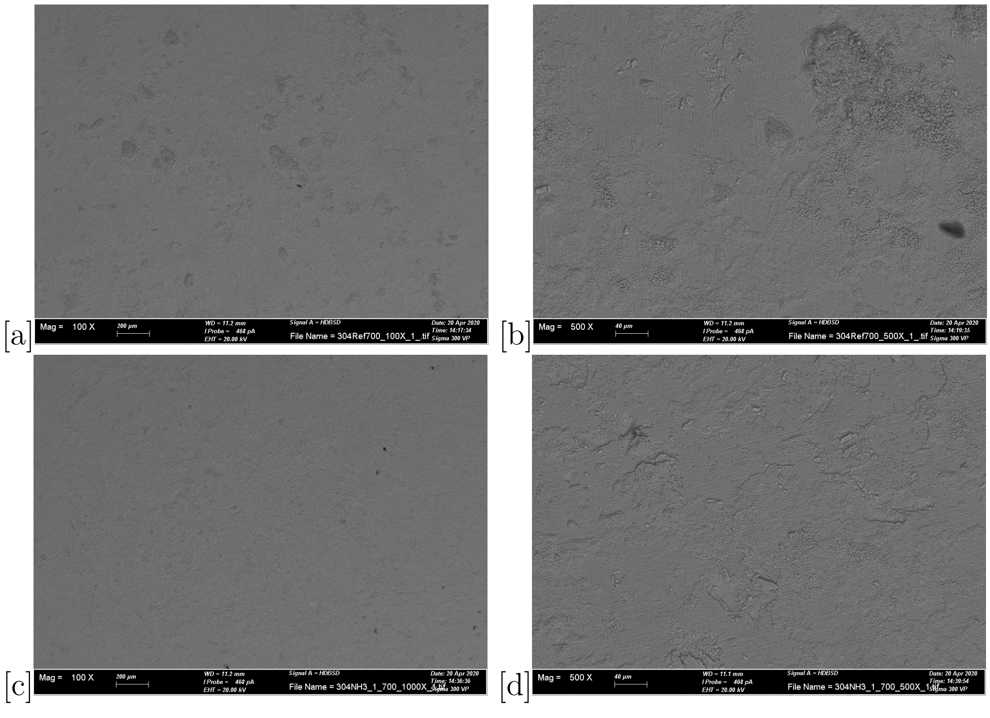

Figure 4.23: a and b are BSD SEM plane view of 1.4307 exposed without ammonia at 700°C for 168h (100x and 550x),c and d are BSD SEM plane view of 1.4307 exposed with ammonia at 700°C for 168h (100x and 550x)

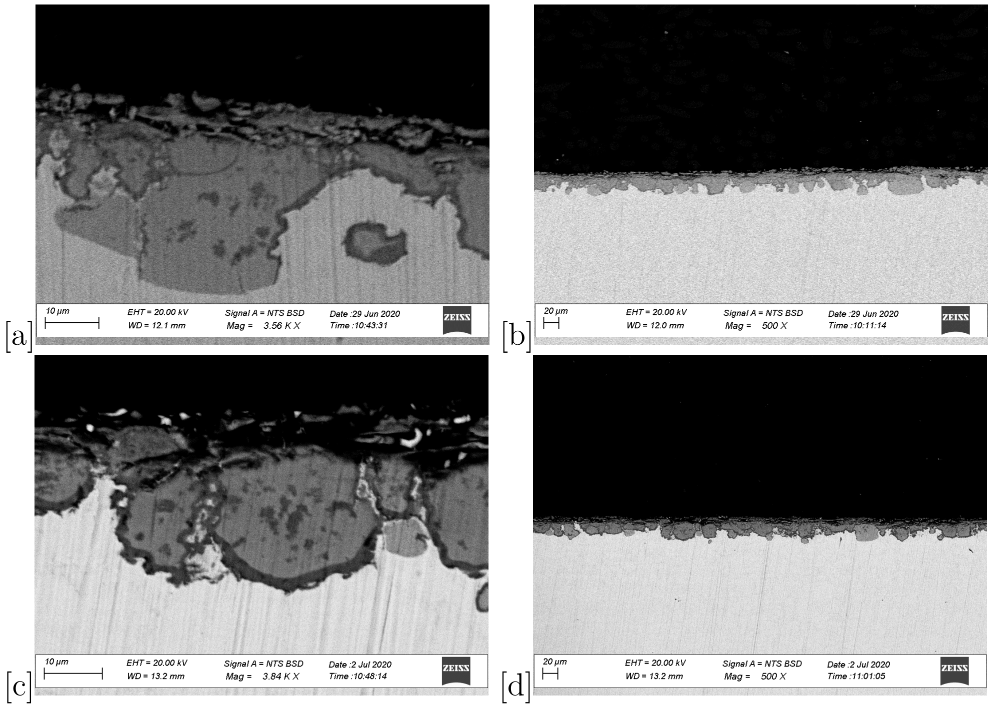

Figure 4.24: a and b are BSD SEM cross section view of 1.4307 exposed without ammonia at 700°C for 168h (3.56Kx and 50x),c and d are BSD SEM cross section view of 1.4307 exposed with ammonia at 700°C for 168h (3.84Kx and 500x)

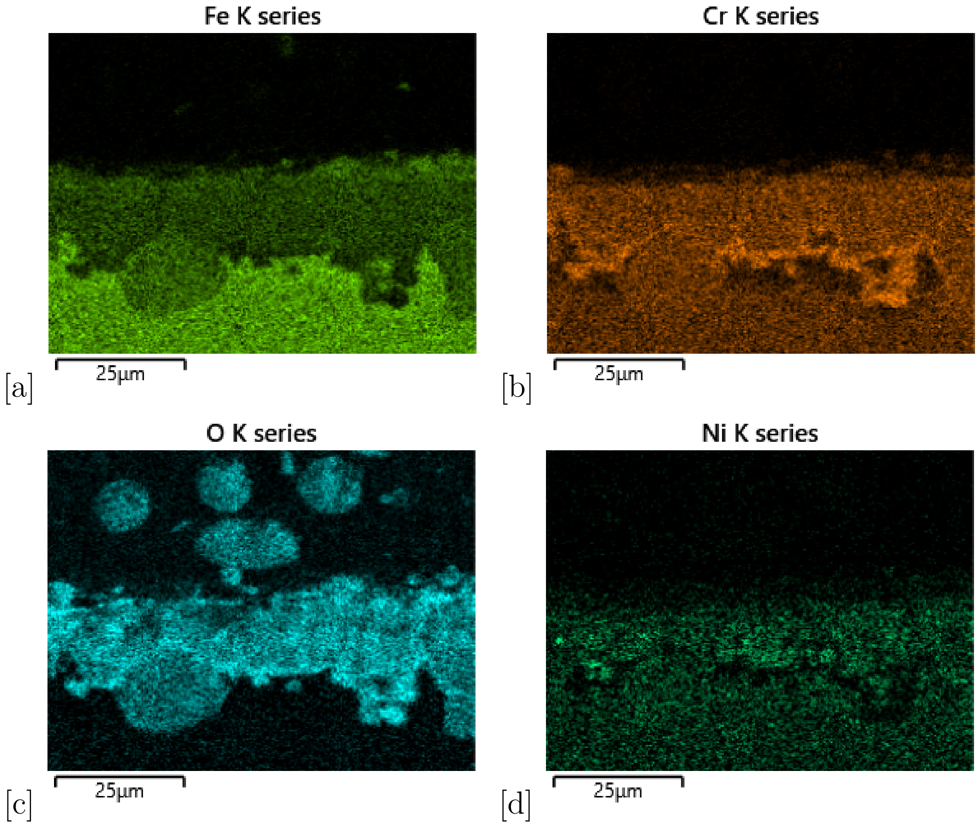

Figure 4.25: Elemental mapping of cross section of 1.4307 exposed without ammonia at 700°C for 168h

The isothermally exposed austenitic 1.4307 sample showed uneven surface in no ammonia atmosphere with large traces of Ni and Cr on the surface.The surface showed iron in the top of the outermost layer,Cr and Ni in the interface between the outermost layer and the inner matrix.It showed a clear view of oxide layer growing inwards.The presence of Ni aids in the oxidation resistance of the material 1.4307 along the Cr.The growth of Chromia scale is influenced by the Si particles in the grain boundary which acts as a diffusion barrier in some places of the scale.Other parts showed that there was no diffusion barrier to stop the growth of chromia scale.The samples in ammonia exposure showed similar behavior compared to the exposure without ammonia.The Chromia scale/ alloy interface showed Cr rich region.The growth of oxide layer was not found to be uniform at inwards.The was observed spallation in the surface as well,which might again be due to thermal stresses created from the atmosphere.The inner Cr rich oxide layer developed the diffusion of Cr into the matrix in some places as the reference exposure.But here the nitrogen signals were identified in the EDS analysis in cross section of the sample.So,1.4307 could possibly allowed the formation of CrN in its matrix itself.

The samples exposed in 550°C (fig.4.22) formed thin oxide layer like 1.4509, but with uniform oxide growth and no spallation.The protective chromium oxide layer was found up to the certain depth from the surface in the ammonia atmosphere sample and reference sample.There were no confirmed signals of nitrogen which tells that there is no nitrogen uptake in this environment.The net mass gain depicts that the sample developed a protective oxide on the surface.

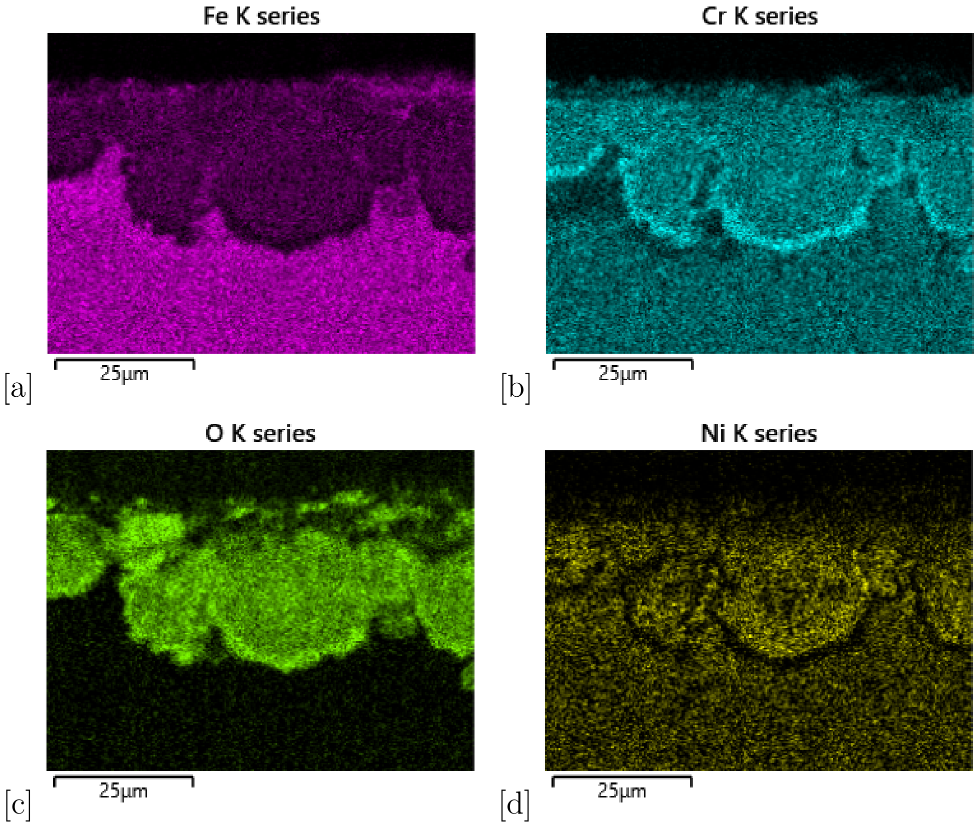

Figure 4.26: Elemental mapping of cross section of 1.4307 exposed with ammonia at 700°C for 168h

4.2.5 1.4404

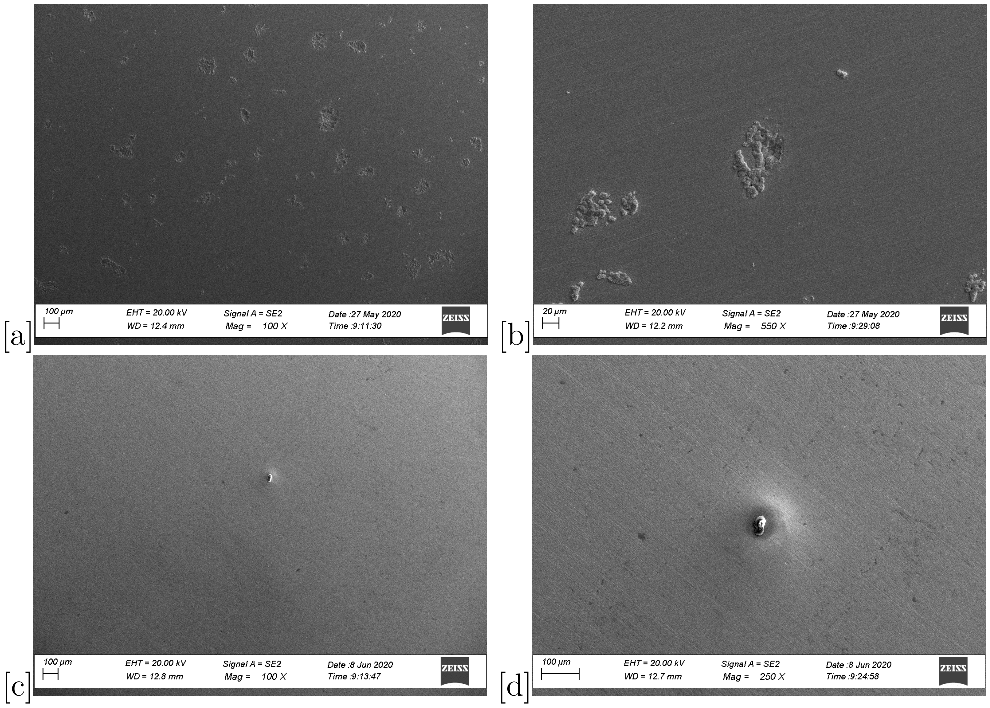

Figure 4.27: a and b are SEM plane view of 1.4404 exposed without ammonia at 550°C for 168h (100x and 550x),c and d are SEM plane view of 1.4404 exposed with ammonia at 550°C for 168h (100x and 250x).

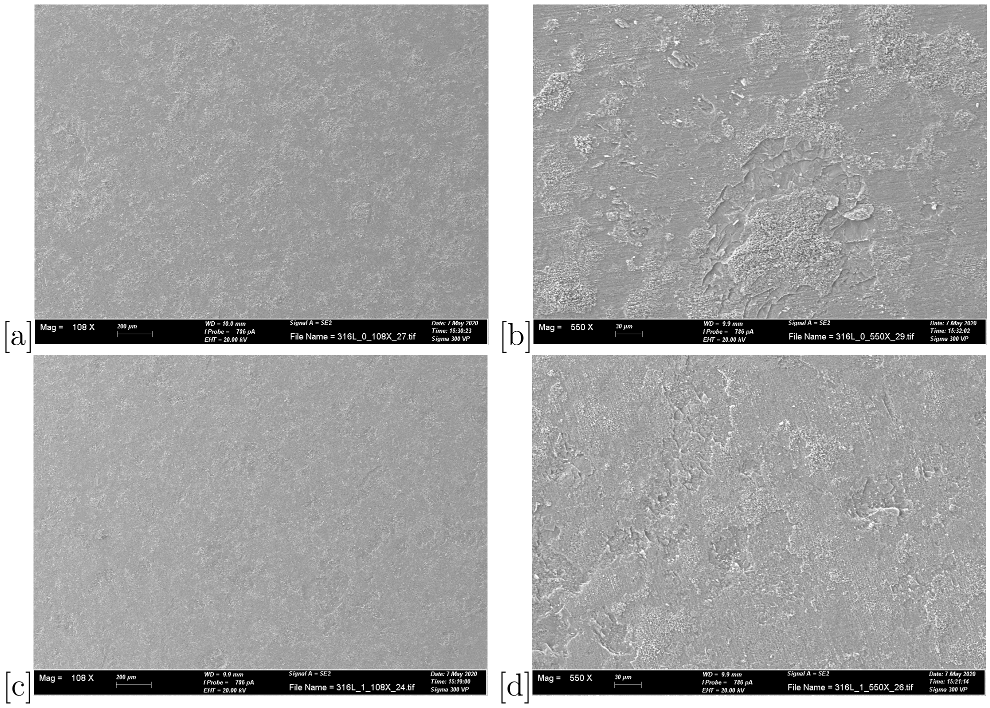

Figure 4.28: a and b are SEM plane view of 1.4404 exposed without ammonia at 700°C for 168h (108x and 550x) using SE detector,c and d are SEM plane view of 1.4404 exposed with ammonia at 700°C for 168h (108x and 550x) using SE detector.

1.4404 (fig.4.27),ferritic wrought stainless steel,showed formation of island like structure of Fe oxide mixed with Ni and Mn on the surface which could be assume be the outer layer.Cr rich mixed oxide was found with uniform morphology at 550°C without ammonia.At ammonia atmosphere,there is uniform thin oxide scale with the composition similar to reference atmosphere (without ammonia).For 700°C (fig.4.28),atmosphere without ammonia shows partially similar to the 550°C sample but in this case,Mo can be seen on the white regions in the SEM image along with Fe,Ni and little amount of Si.The darker region have less amount of S as well.The oxide layer was thick and spallation occurred at 700°C.

4.2.6 SiMo51

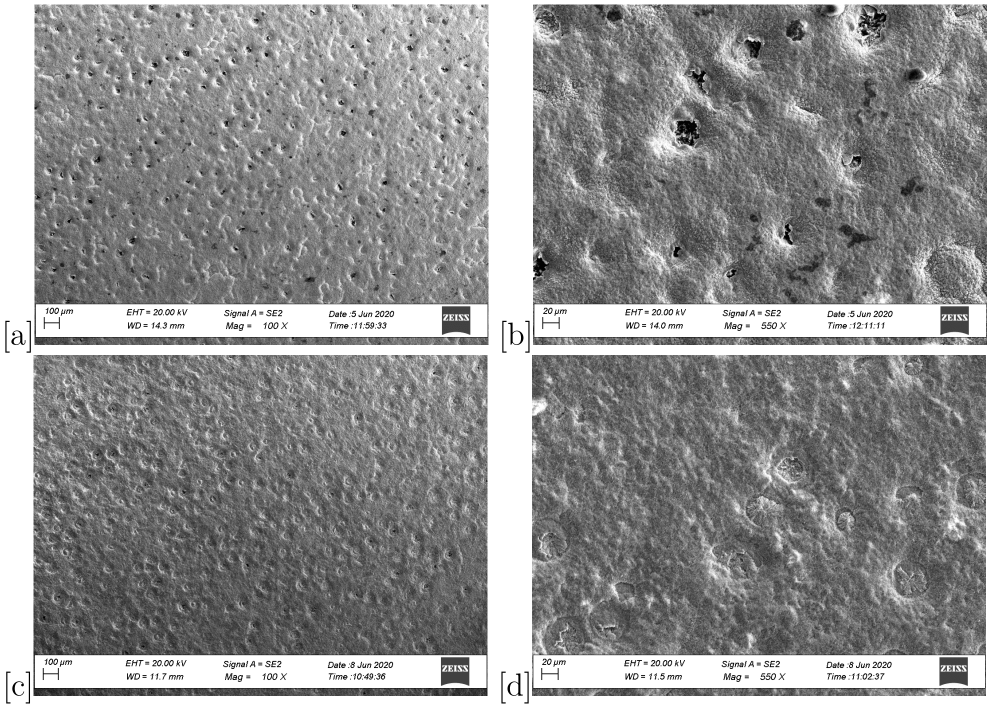

Figure 4.29: a and b are SEM plane view of SiMo51 exposed without ammonia at 550°C for 168h (100x and 550x),c and d are SEM plane view of SiMo51 exposed with ammonia at 550°C for 168h (100x and 550x)

SiMo51 (fig.4.29) at 550°C shows graphite nodules on the surface but the nodules are oxidised in ammonia atmosphere samples.Both the samples did not have any oxidation products spalled off.For 700°C,there was very little spallation in reference and ammonia atmosphere samples.The graphite nodules observed to be oxidised in ammonia atmosphere similar to 550°C.Ferrite (white area in fig.4.30) is seen in ammonia sample.At both the temperatures,surface morphology was not even;despite 550°C having thin oxide layer.The scale contains Fe oxide mixed with Si and Mo.Fig.4.31 shows the cross section of SiMo51 in both the atmospheres at 700°C.The spheroidal graphite nodules and ferrite are seen in oxide scale and the matrix as well.The formed oxide scale is porous and have cracks in it.The formed scales is not so denser compared to wrought materials like 1.4509 and 1.4307 and there is not inward diffusion of the oxide scale.

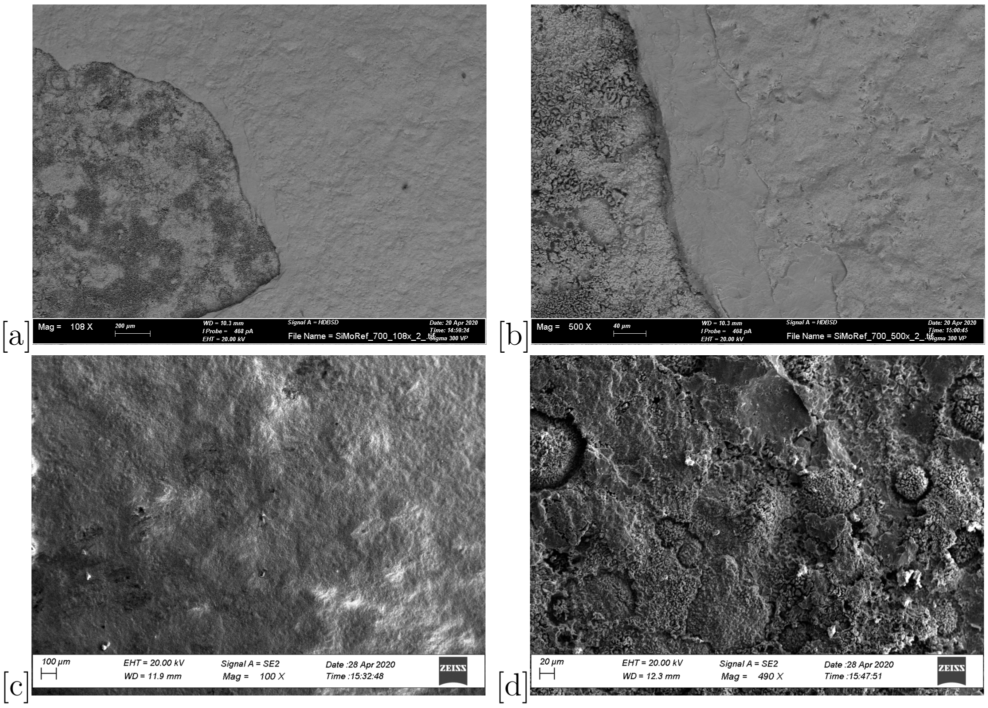

Figure 4.30: a and b are BSD SEM plane view of SiMo51 exposed without ammonia at 700°C for 168h (108x and 550x),c and d are SEM plane view of SiMo51 exposed with ammonia at 700°C for 168h (100x and 490x)

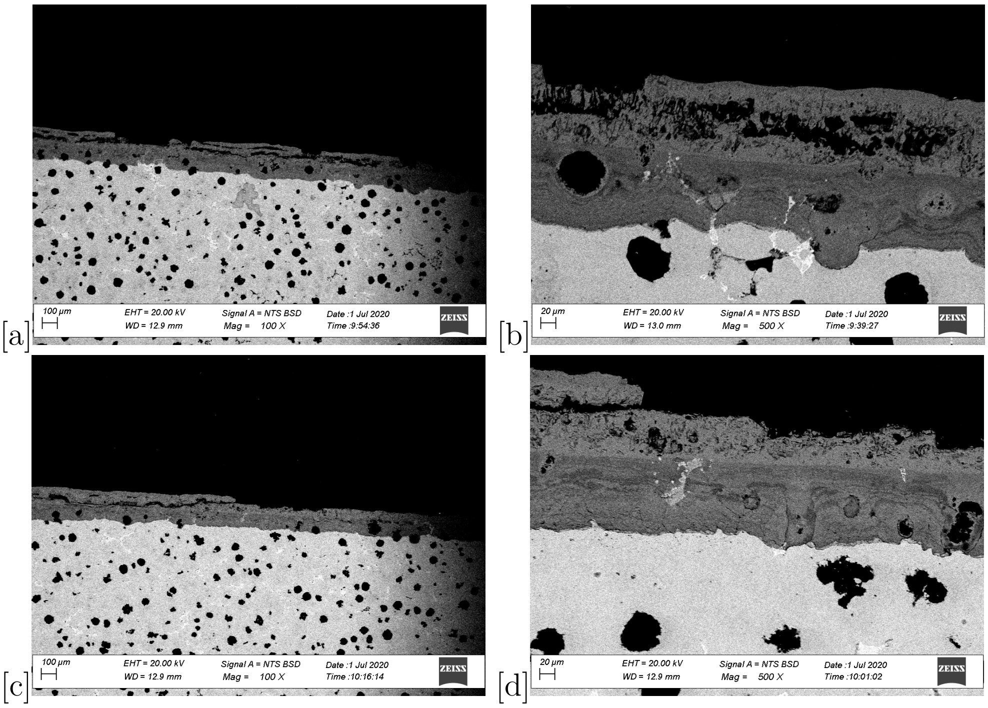

Figure 4.31: a and b are BSD SEM cross section view of SiMo51 exposed without ammonia at 700°C for 168h (100x and 500x),c and d are BSD SEM cross section view of SiMo51 exposed with ammonia at 700°C for 168h (100x and 500x)

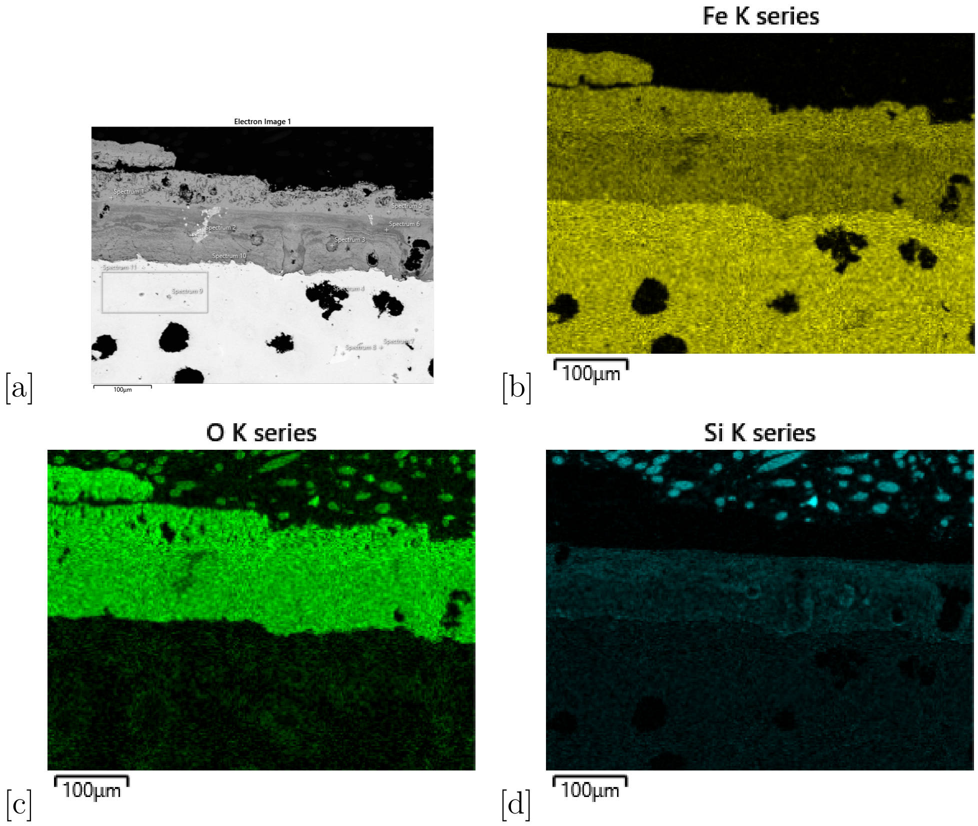

Figure 4.32: Elemental mapping of cross sectioned SiMo51 with ammonia at 700°C for 168h.

4.2.7 HK30

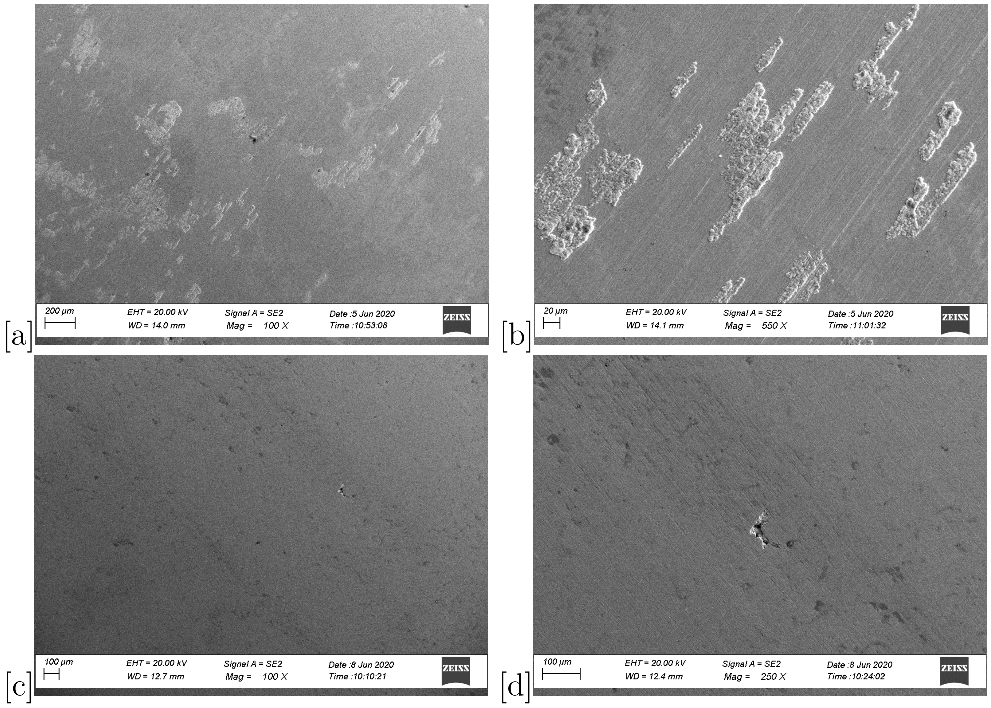

Figure 4.33: a and b are SEM plane view of HK30 exposed without ammonia at 550°C for 168h (100x and 500x),c and d are SEM plane view of HK30 exposed with ammonia at 550°C for 168h (100x and 250x)

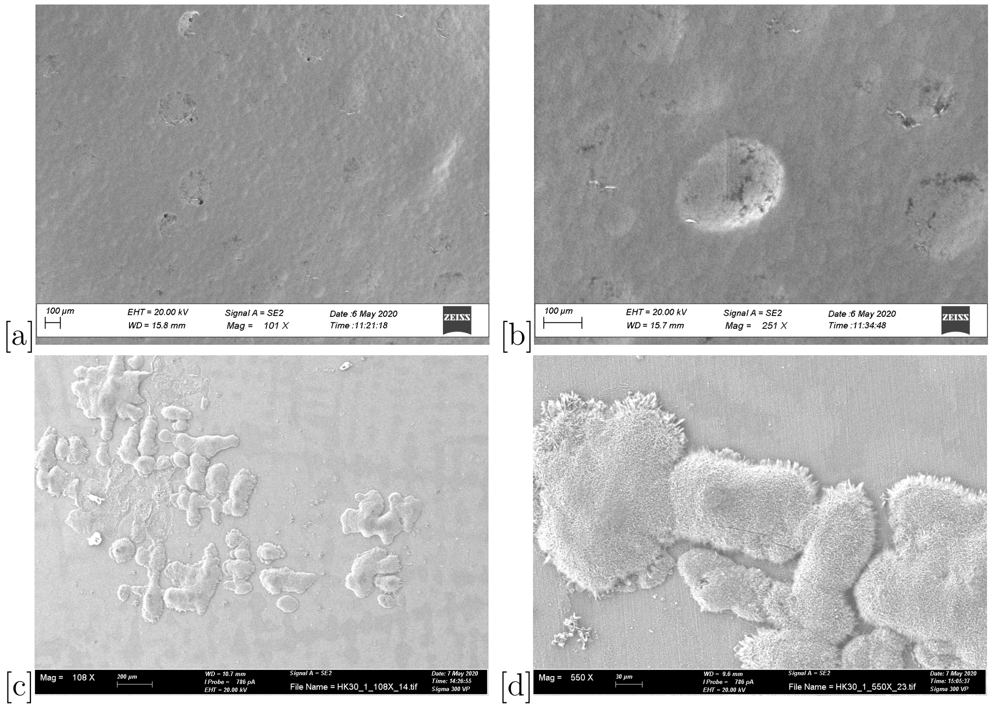

Figure 4.34: a and b are SEM plane view of HK30 exposed without ammonia at 700°C for 168h (101x and 251x) using SE detector,c and d are SEM plane view of HK30 exposed with ammonia at 700°C for 168h (108x and 550x) using SE detector.

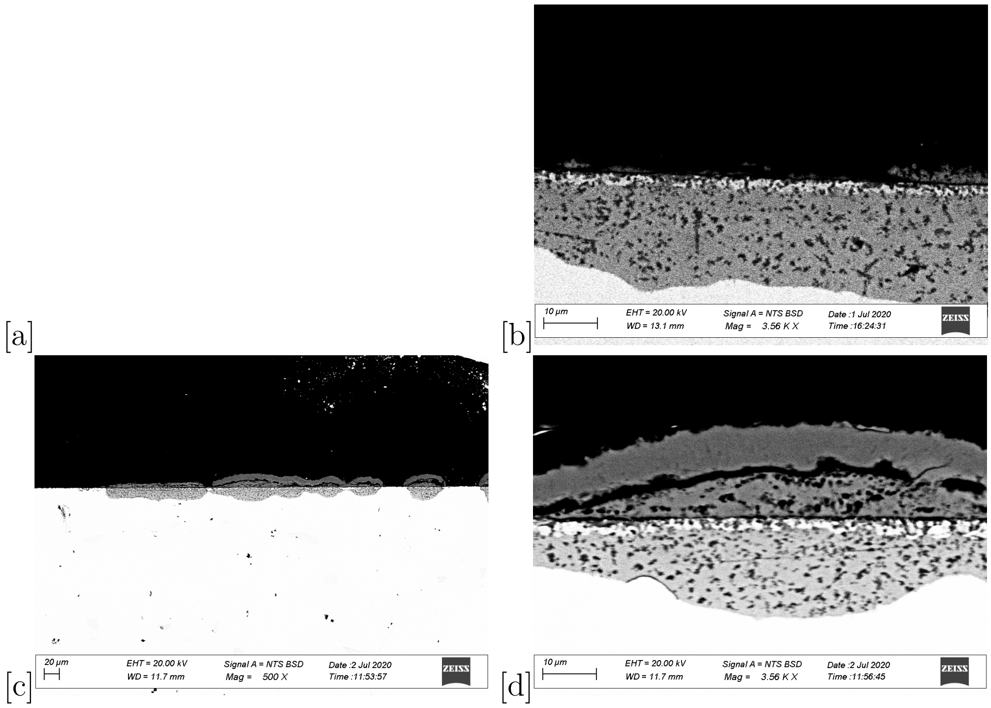

Figure 4.35: a and b are SEM cross section view of HK30 exposed without ammonia at 700°C for 168h (101x and 251x) using back scattered electron detector,c and d are SEM cross section view of HK30 exposed with ammonia at 700°C for 168h (108x and 550x) using back scattered electron detector.

HK30, austenitic cast stainless steel, is always considered a high temperature behavior material when comparing to other candidate materials. It showed the formation of iron oxide on the surface along the dendrites. This iron oxide has few cracks on them along the needle like structure. The manganese was in more amount on the surface with Cr_2O_3 forming a spinel phase which could be detrimental in high temperature applications especially in ammonia atmosphere. The manganese is more stable comparing to Cr_2O_3.The cross section formed Fe oxide on top and Ni below on the surface and the inward diffusion of Cr is seen in both the atmospheres.The formed scale has very fine cracks in it which is observed in SEM plane view as well (fig.4.33.d).There are traces of N in the matrix which could the alloying element from casting process.

4.2.8 SiMo51 coated

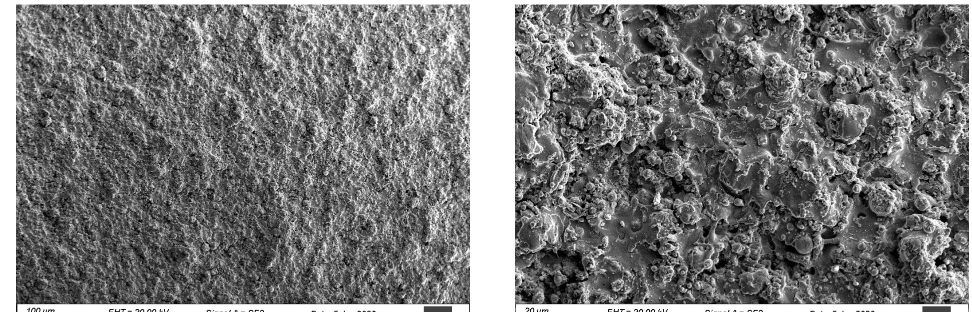

Figure 4.36: a and b are SEM plane view of SiMo51 coated exposed without ammonia at 550°C for 168h (100x and 550x) using SE detector,c and d are SEM plane view of SiMo51 coated exposed with ammonia at 550°C for 168h (100x and 550x) SE detector.

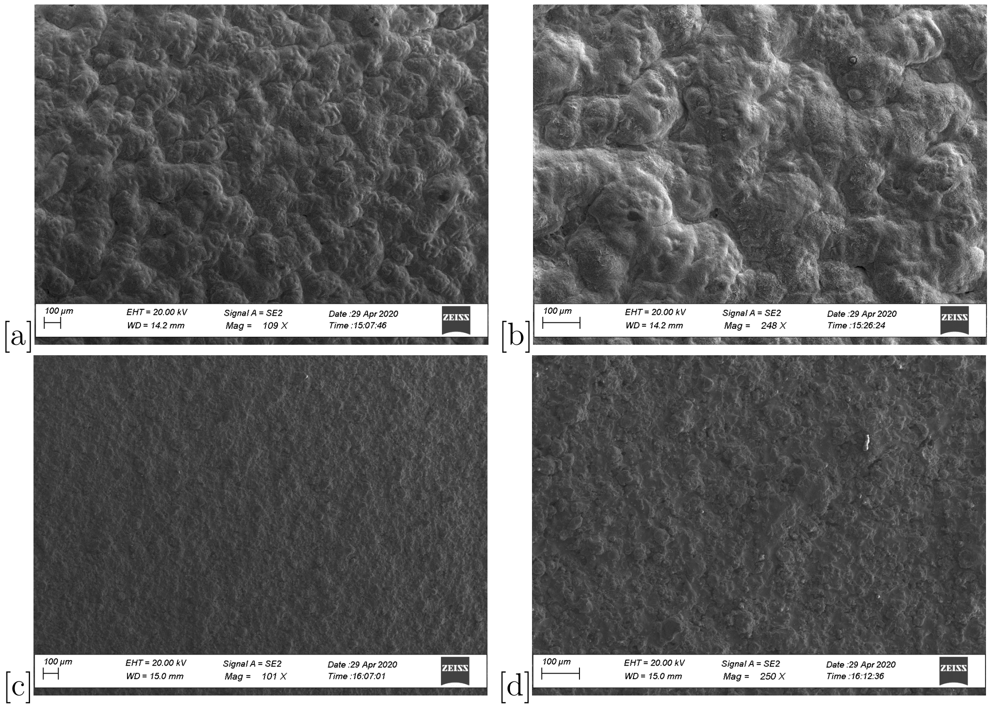

Figure 4.37: a and b are SEM plane view of SiMo51 coated exposed without ammonia at 700°C for 168h (100x and 250x),c and d are SEM plane view of SiMo51 coated exposed with ammonia at 700°C for 168h (101x and 250x)

In this material,in both the atmosphere and temperature,no spallation occurred.The surface is wrinkled and rough where the outermost coating layer was found unaffected after the ammonia exposure.The formation of Fe oxide mixed with Si,Mn,Mo and Ni is found in both the temperatures.Ni content may be from the coating composition.

4.2.9 713C

In 713C(fig.4.37),unlike other materials Ni content is higher and it may form NiO_2. Further analysis using XRD,the crytal structure can be concluded.This alloy has the possibility to form Alumina which is better protective than SiO_2.At 700°C,the grinding marks are not seen,meaning that the oxide layer is thick comparing to the sample from 550°C.Despite this dissimilarity,the NiO_2 is formed along the grain boundaries.Alloying of this material makes it very expensive but it is well suited for the high temperature applications.

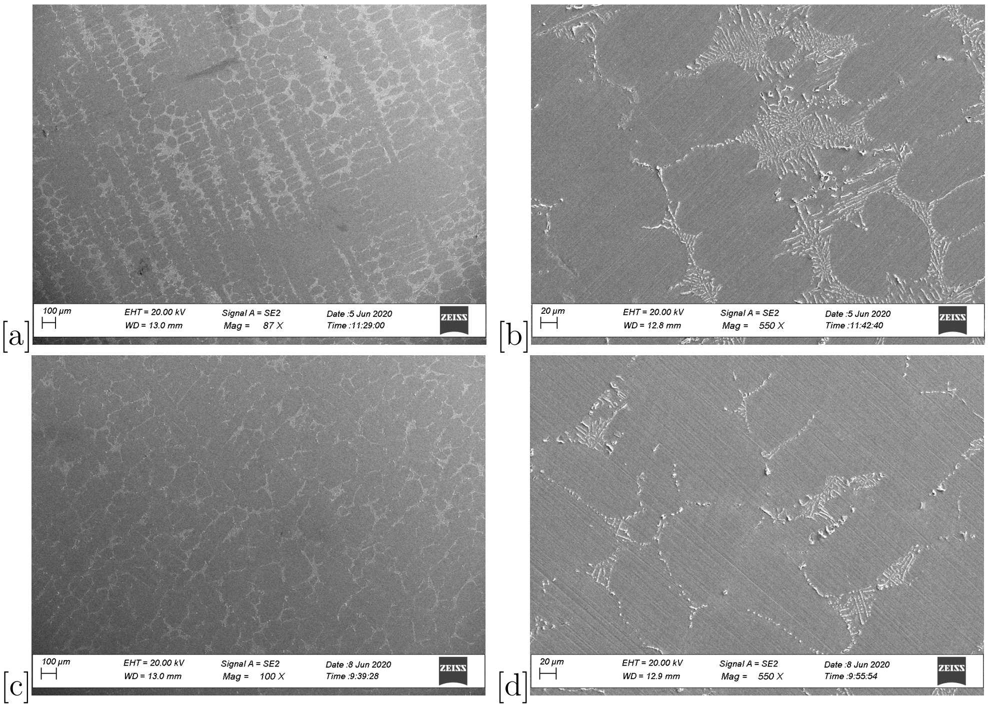

Figure 4.38: a and b are SEM plane view of 713C exposed without ammonia at 550°C for 168h (100x and 550x),c and d are SEM plane view of 713C exposed with ammonia at 550°C for 168h (100x and 550x)

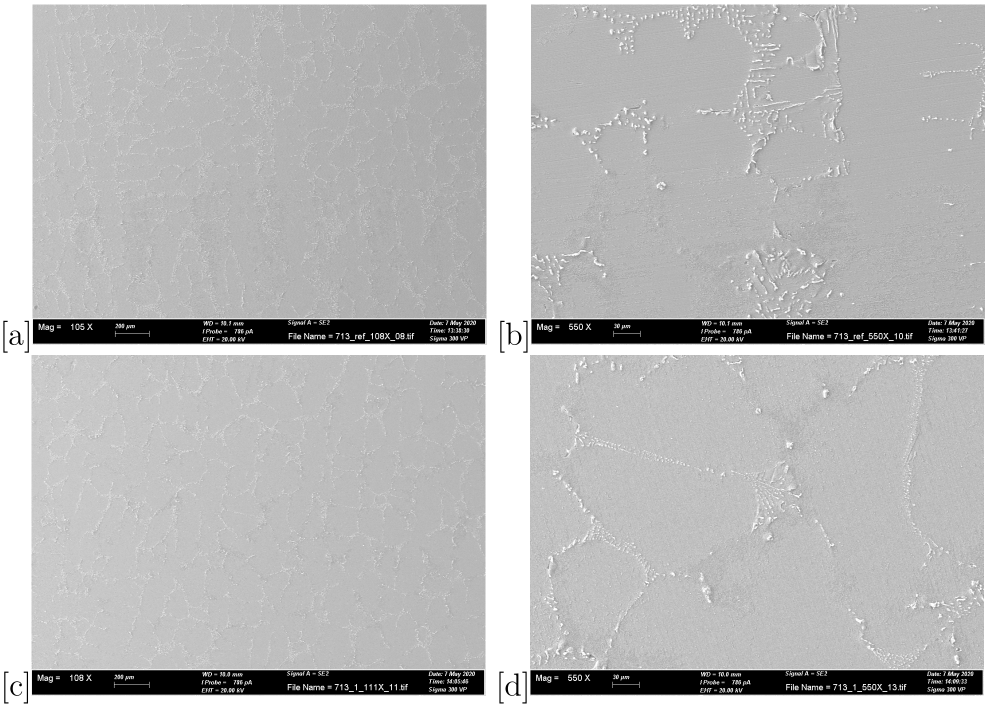

Figure 4.39: a and b are SEM plane view of 713C exposed without ammonia at 700°C for 168h (108x and 550x),c and d are SEM plane view of 713C exposed with ammonia at 700°C for 168h (111x and 550x)

4.3 X-ray Diffraction (XRD)

The XRD peaks where analysed for all the samples in both the temperatures and atmospheres.Preferably,M_2O_3 which might be hematite and eskolite while ,M_3O_4 as magnetite was selected; considering this could be protective at higher temperature with corrosive environment.Hematite is more stable phase than magnetite at medium range temperature and high oxygen activity whereas magnetite is stable at lower oxygen activity.Most of the materials used in this thesis work showed aforementioned iron oxides in both temperatures.Figure 4.40 and 4.41 shows the XRD crystal structures for the candidate materials and alloy presence.The circled M_2O_3 depicted the strong presence as iron oxides.

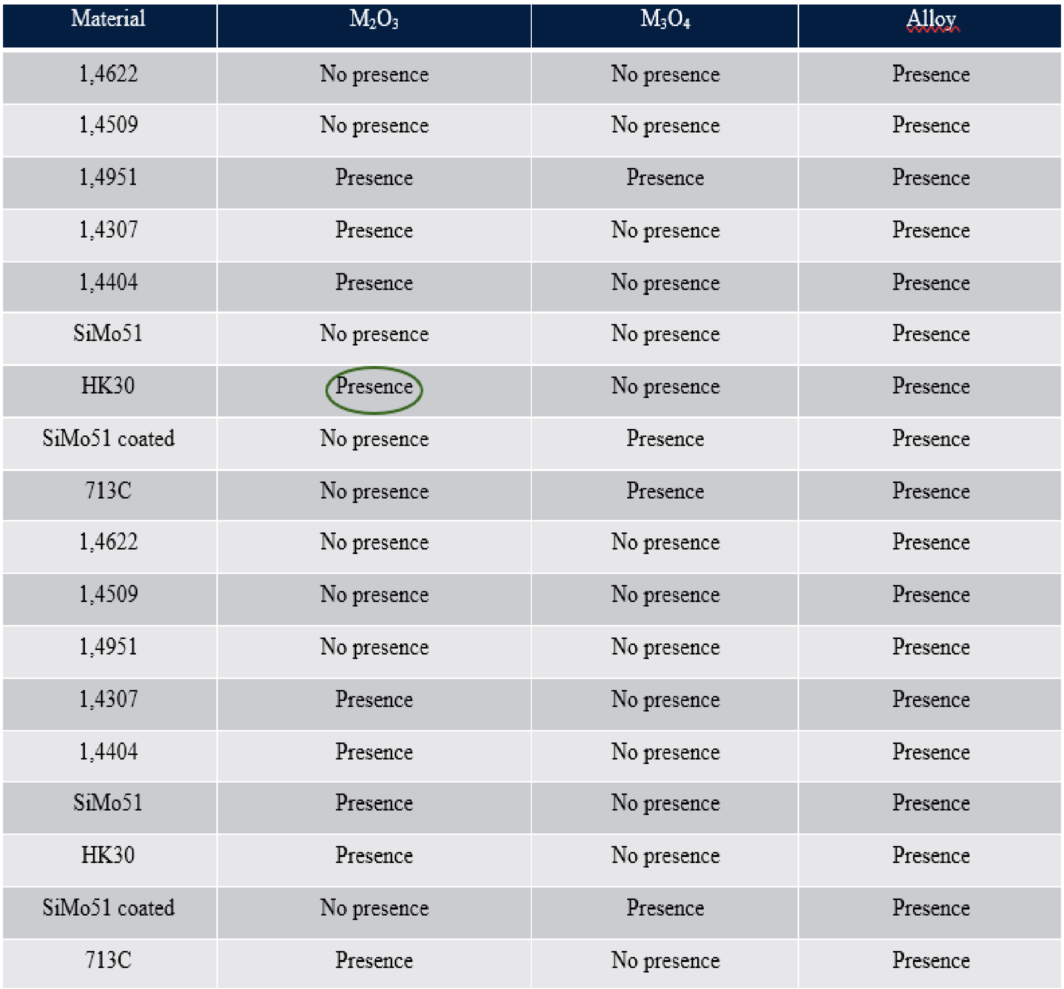

Material	M_2O_3	M_3O_4	Alloy
1,4622	No presence	No presence	Presence
1,4509	No presence	No presence	Presence
1,4951	Presence	Presence	Presence
1,4307	Presence	No presence	Presence
1,4404	Presence	No presence	Presence
SiMo51	No presence	No presence	Presence
HK30	Presence	No presence	Presence
SiMo51 coated	No presence	Presence	Presence
713C	No presence	Presence	Presence
1,4622	No presence	No presence	Presence
1,4509	No presence	No presence	Presence
1,4951	No presence	No presence	Presence
1,4307	Presence	No presence	Presence
1,4404	Presence	No presence	Presence
SiMo51	Presence	No presence	Presence
HK30	Presence	No presence	Presence
SiMo51 coated	No presence	Presence	Presence
713C	Presence	No presence	Presence

Figure 4.40: XRD peaks of exposure with no ammonia and 1%NH_3 at 550°C for 168h.

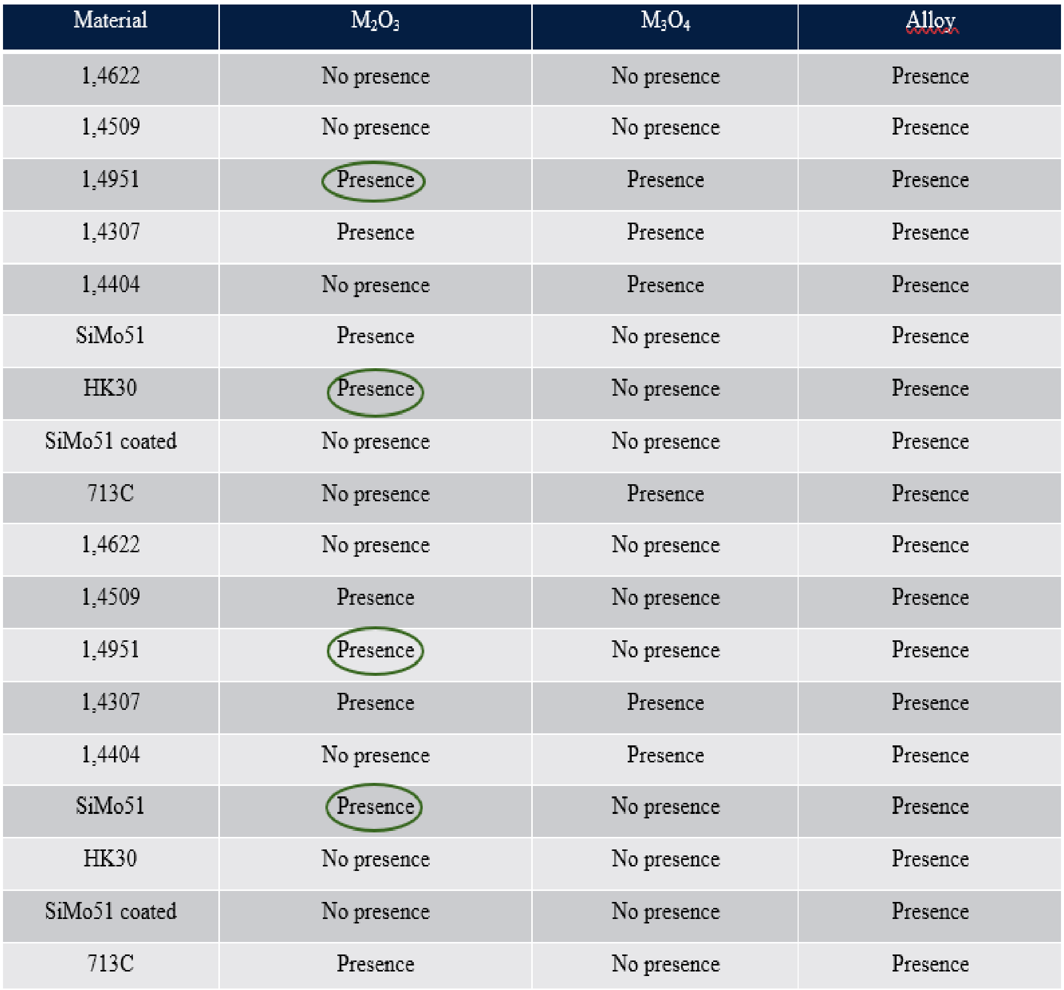

Material	M_2O_3	M_3O_4	Alloy
1,4622	No presence	No presence	Presence
1,4509	No presence	No presence	Presence
1,4951	Presence	Presence	Presence
1,4307	Presence	Presence	Presence
1,4404	No presence	Presence	Presence
SiMo51	Presence	No presence	Presence
HK30	Presence	No presence	Presence
SiMo51 coated	No presence	No presence	Presence
713C	No presence	Presence	Presence
1,4622	No presence	No presence	Presence
1,4509	Presence	No presence	Presence
1,4951	Presence	No presence	Presence
1,4307	Presence	Presence	Presence
1,4404	No presence	Presence	Presence
SiMo51	Presence	No presence	Presence
HK30	No presence	No presence	Presence
SiMo51 coated	No presence	No presence	Presence
713C	Presence	No presence	Presence

Figure 4.41: XRD peaks of exposure with no ammonia and 1%NH_3 at 700°C for 168h.

4.4 Glow-Discharge Optical Emission Spectroscopy (GD-OES)

GD-OES revealed the elemental composition in the surface of the samples exposed at 550°C for 168h in the simulated gas atmosphere with 5%O_2+10%CO_2+10%H_2O+N_2 +1%NH_3.Thin oxide film was developed in all the candidate materials in ammonia and reference atmosphere at both the temperatures.The graph shows the elemental composition of Cr,Mn,Si,O,Fe and Ni in the surface,sub-surface and alloy.Materials such as HK30 and 1.4307 showed good traces of Cr on the surface.Oxygen activity on surface 5%O_2 and near the interface of oxide film and the metal 2%O_2 can be known from the obtained graphs.The graphs are included in the appendix for further reference.

5

Discussion

5.1 Effect of temperature on the materials

The temperature influence is the most important factor to be considered while selecting the materials for exhaust line applications.In this study different materials have been investigated in 700°C and 550°C.High temperature corrosion testing in the above-mentioned temperatures showed difference in their oxidation behavior where some alloys showed internal oxidation and severe spallation and others showed formation of protective oxide layer.The temperature 700°C showed more spallation in all the candidate material, meaning that the outer M_3O_4 oxide in most of the sites and M_2O_3 oxide in very few sites could have fallen off and new layer would have grown for example,called as healing layer.At the same time,at 550°C the oxide scale was adherent to the alloy showed by mass calculations,optical inspection and GD-OES (a mean value of the entire surface).

In this study,the protective chromia layer was observed at 550°C while 700°C had porous Fe oxide on top. Also,Si was embedded in iron oxide matrix at 700°C in 1.4509, SiMo51,SiMo51 coated and in HK30.Eventually,these Si particles in iron oxide matrix could have spalled off because of the reaction with the oxidation species like water and CO_2.The reason that the protective silica layer was not formed as the diffusion Si is low at lower temperatures.This is like the study by Tholence [20];where protective chromia layer was not observed in 850°C and 950°C.

5.2 Effect of different atmospheres on the materials

In this study,the samples were exposed in exhaust atmosphere containing $5\%O_2$, $10\%H_2O$, $10\%CO_2$, N_2,$1\%NH_3$.The presence of water vapor in the atmosphere had effect on the oxidation capability of the chromia forming materials,by promoting the oxidation rate in high Cr alloyed materials like 1.4307,1.4951 and HK30;which is assumed to have led to chromium depletion in inner layer,as studied by Ekstrom et,al.[4].The small effect by Nb and C,which was also observed in the oxide scale;presence of Nb could act as a crack initiation site where the oxidation species can pass through, eventually the spallation of oxide scale. (Ref3) As mentioned above,the presence of H_2O and CO_2 could break away the healing layer with Si particles by oxygen transport.The samples exposed in ammonia atmosphere showed comparatively less spallation to the reference atmosphere which led to the formation of uniform oxide scale of M_3O_4 outer layer and M_2O_3 inner layer as shown in SEM images.

HK30 exposed in ammonia showed the traces of N particles below the inner Cr rich layer;the composition of the bulk material itself was with N content probably due to casting process for the latter.The presence of N in bulk may lead to severe degradation of mechanical properties when exposed to long term oxidation at higher temperatures.The N rich ammonia environment showed some favorable scale formation such as magnetite and chromia(in-homogeneous) on the surface without spalling off.

5.3 Comparison to wrought and cast materials

The grain size in wrought materials are the important factor for their corrosion resistance.They have smaller grain size which cause the formation of chromia scale faster.This might be aided by rapid Cr diffusion and very little lateral distance for the oxide to grow [38].The cast materials had defects and carbides might influence the oxidation resistance.The wrought material contains very less carbon which leads to less formation of carbides and higher percent of protective species such as Cr than the cast materials.The general behaviour of the wrought material in terms of spallation (mass change) was much better than its cast counterpart in both the exposures with ammonia and without ammonia.

The cast material for example,SiMo51 showed more spallation in 700°C than in 550°C which might be because of the higher carbon content and low content of Cr.Despite having Si of about 4wt%,this material hardly developed the healing layer after the spallation which might have led to the formation of non-protective oxide scale.When comparing SiMo51 and 1.4509 (a wrought ferrite material with higher Cr content),the latter had less spallation in both the temperatures with ammonia and without ammonia because the formed oxide scale was thin and had stable growth.Hematite was developed in the outer layer and mixed Chromia scale in the inner layer.Additionally,it is assumed that carburization effect could have occurred on the surface and this might have been surpassed by the including Mn to form manganese spinel which act as a barrier to carbon transmission and metal-oxygen diffusion [39].Despite the worst behaviour of cast iron materials in certain aspects like casting defects and inclusions,it can be used for higher temperature applications because of its economically cheap and the composition can be changed accordingly to the applications.

5.4 Behaviour of Ferritic and austenitic stainless steels

Ferrite materials have lower thermal expansion coefficient comparing to austenite materials [20].Austenite is the high temperature phase with face centered cubic crystal structure and alpha phase is the ferrite with body centered cubic structure which is beneficial to Cr diffusion in the matrix because of higher diffusion coefficient [40].Austenite materials have Ni to stabilize them at the room temperature and for higher temperature applications additional alloying elements like higher percent of Cr,Mn and Si are included to obtain a protective oxide layer in harsh environments like ammonia.The ferrite to austenite transformation usually occurs at the range of 850°C.In this study,HK30 an austenite behaved good by developing outer hematite with Ni on the top and inner mixed metal oxide with M_2O_3 composition and showing no spallation in both the temperatures with ammonia and without ammonia.Even though they showed no spallation,internal oxidation was observed in the material which could lower the mechanical properties.While considering ferritic materials,unlike SiMo51 and SiMo51 coated,the ferritic grade stainless steel materials showed very less spallation at 700°C and no spallation at 550°C.For example,1.4509 developed outer hematite layer which comparatively behaves well as a protective oxide and inner mixed Chromia (which is assumed to be Chromia scale) might be protective.When considering the silica layer,very less materials showed even scale in both the temperature particularly ferrite.However,the ferritic grades showed very little traces of silica particles (probably SiO2) in the inner layer due to the lack of ability to form protective Chromia (less Cr content).With regard to the behavior in severe corrosive environment with high temperature, wrought austenite materials could be used due to their higher Cr content for better corrosion resistance and higher Ni content to have better surface quality.

6

Conclusion

By using simulated exhaust gas in a furnace, there was observed severe influence of ammonia along with water vapour,CO_2 and O_2 onto the surface of the candidate materials in higher temperature nitrogen uptake in oxidation environment.The aim of this thesis work was to study the growth of protective oxide scale formation in ammonia environment and reference environment without ammonia.Isothermal exposure was used to study the different oxides formed on the metal and their behaviour over the long-haul oxidation process.They formed protective Fe rich oxide like Hematite and Cr rich chromia scale(inhomogeneous) were shown in the ammonia environment.However,no materials showed continuous thin oxide scale growth rather thick oxide scale because of rapid oxidation was observed in higher temperature which resulted in the spallation.Austenite materials had internal oxidation effect which might reduce the mechanical properties at higher temperature applications for example,HK30.The cast materials showed more oxidation may be because of higher content of carbides than their wrought counterparts.When selecting the materials for exhaust system applications,there are several other factors such as mechanical properties,cost,thermal coefficient to be considered apart from their corrosion resistance.Sustainable material selection using Life cycle analysis could be used to get the better material choice to reduce emission.

7

Future work

With this study on high temperature corrosion at urea dosage, there are some suggestions for further study of the material's behavior in high temperature corrosive environment with the exhaust gas mixture.The oxide scale thickness can be measured in-order to know the scale thickness which will be useful to optimize the engine working conditions and urea dosage.The exposure could be as long-term, for example 1000h cyclic exposure.This might help to understand the oxide scale behavior in more detail.While the long-term oxidation process, focusing on other mechanical deformations like fatigue of the materials during in-service condition, stress corrosion cracking could be helpful in selecting the materials.

Additional care shall be given to the metallography as it is a most important part which also determines the oxide scale growth and microstructure behaviour.Furthermore,the alumina forming materials can be used to have some reliable performance at higher temperatures and are impermeable in water containing environment.

Bibliography

[1] 2012. Sweden's Environmental Objectives. Stockholm: Swedish Environmental Protection Agency.

[2] Saedlou, S., Santacreu, P. and Leseux, J., 2011. Suitable Stainless Steel Selection for Exhaust Line Containing a Selective Catalytic Reduction (SCR) System. SAE Technical Paper Series,.

[3] Corrosionsource.com. 2020. Important Issues In High Temperature Corrosion - Nitridation. [online] Available at: <https://www.corrosionsource.com/FreeContent/1/Important+Issues+in+High+Temperature+Corrosion+-+ Nitridation> [Accessed 4 May 2020].

[4] M. Ekström, P. Szakalos and S. Jonsson, "High-temperature corrosion of materials for cast exhaustcomponents", 2014. Available: http://eurocorr.efcweb.org/2014/abstracts/14/7383.pdf. [Accessed 4 May 2020].

[5] 2012. Corrosion Of Metals And Alloys — Test Method For Isothermal-Exposure Oxidation Testing Under High-Temperature Corrosion Conditions For Metallic Materials. 1st ed. International standards organization, p.14.

[6] Lai, G., 1990. High temperature corrosion of engineering alloys. ASM international,.

[7] Lai, G., 2006. Corrosion in High-Temperature Environments. Corrosion: Environments and Industries, pp.754-761.

[8] En.wikipedia.org. 2020. Exhaust System. [online] Available at: <https://en.wikipedia.org/wiki/Exhaust system> [Accessed 10 May 2020].

[9] Aniekan E., I., Ejiroghene Kelly, O. and Abdulsamad, G., 2017. Engineering Material Selection for Automotive Exhaust Systems Using CES Software. International Journal of Engineering Technologies IJET, 3(2), pp.50-60.

[10] Ross, J., 2019. How Does a Catalyst Work?. Contemporary Catalysis, pp.69-89.

[11] 2020. Air Pollution Control Technology Fact Sheet. United states Environmental protection agency.

[12] Nockert, J. and Norell, M., 2011. Corrosion at the urea injection in SCR-system during component test. Materials and Corrosion, 64(1), pp.34-42.

[13] R. Crane and P. Wisby, "Light-duty diesel exhaust after-treatment by a multicyclone particulate separator with an oxidation catalyst", Proceedings of the Institution of Mechanical Engineers, Part D: Journal of Automobile Engineering, vol. 214, no. 7, pp. 741-749, 2000.

[14] Shu, G., Hu, C., Tian, H., Li, X., Yu, Z. and Wang, M., 2019. Analysis and Optimization of Coupled Thermal Management Systems Used in Vehicles. Energies, 12(7), p.1265.

[15] Sun, Z., Wang, X., Wang, X. and Zhou, J., 2017. Combustion and emission analysis of heavy-duty vehicle diesel engine.

[16] Khanna, A., n.d. Fundamentals of high temperature oxidation/corrosion. In: ASM International.

[17] Ekström, M., 2015. Oxidation and corrosion fatigue aspects of cast exhaust manifolds.Doctoral thesis.KTH Royal Institute of Technology.

[18] Khanna, A., n.d. Fundamentals of High Temperature Oxidation/Corrosion.

[19] Yepez, Omar. (2018). On the Mechanism of High Temperature Corrosion.

[20] Tholence, F., Norell, M. (2005). Nitride precipitation during high temperature corrosion of ductile cast irons in synthetic exhaust gases. Journal Of Physics And Chemistry Of Solids, 66(2-4), 530-534. Retrieved 11 August 2020, from.

[21] Lai, G. (2007). Chapter 3 - Oxidation. In High-Temperature Corrosion and Materials Applications, ASM International (pp. 5-66). ASM international. Retrieved 12 August 2020, from.

[22] Fukumoto, Michihisa Akabori, Kouta Sonobe, Hiroshi Hara, Motoi. (2017). Investigation of High Temperature Oxidation in Steam for Fe-Cr Alloy Using the Combination of a Hydrogen Sensor and an Oxygen Pump-Sensor. Journal of the Japan Institute of Metals. 81. 408-416. 10.2320/jinstmet.JB201701.

[23] Kaya, K., Hayashi, S., Ukai, S. (2014). High-temperature Oxidation Behavior of 9Cr Ferritic-steel in Carbon Dioxide. ISIJ International, 54(6), 1379-1385. https://doi.org/10.2355/isijinternational.54.1379

[24] Evans, H., Donaldson, A., Gilmour, T. (1999). Oxidation Of Metals, 52(5/6), 379-402. https://doi.org/10.1023/a:1018855914737

[25] Col, A., Parry, V., Pascal, C. (2017). Oxidation of a Fe–18Cr–8Ni austenitic stainless steel at 850°C in O2: Microstructure evolution during breakaway oxidation. Corrosion Science, 114, 17-27. https://doi.org/10.1016/j.corsci.2016.10.029

[26] Cortie, M., du Toit, M. (2016). Stainless Steels, Ferritic. Reference Module In Materials Science And Materials Engineering. https://doi.org/10.1016/b978-0-12-803581-8.02501-7

[27] Elger, R. (2016). High temperature corrosion in biomass-fired energy appliacations (Ph.D,). KTH Royal institute of Technology.

[28] Weronski, A., Hejwowski, T. Thermal fatigue of Metals (pp. 113-115). Marcel Dekker Inc.

[29] Xiang, S. (2018). High-Temperature Corrosion-Fatigue of Cast Alloys for Exhaust Manifolds (Licentiate Thesis). KTH Royal Institute of Technology.

[30] Mola, R., Bucki, T. and Wcislo, K., 2014. Characterization ofCoatingson Grey Cast IronFabricated by Hot-dippingin Pure Al, AlSi11 and AlTi5 Alloy. ARCHIVES of FOUNDRY ENGINEERING, 14(1/2014), pp.85-90.

[31] University of Glasgow - Schools - School of Geographical Earth Sciences - Research - Research facilities - ISAAC : Imaging Spectroscopy and Analysis Centre - Services - Scanning Electron Microscopy. (2020). Retrieved 4 August 2020, from https://www.gla.ac.uk/schools/ges/research/researchfacilities/isaac/services/scanningelectronmicroscopy/

[32] Nanoscience Instruments. 2020. Scanning Electron Microscopy - Nanoscience Instruments. [online] Available at: <https://www.nanoscience.com/techniques/scanning-electron-microscopy/> [Accessed 24 May 2020].

[33] Andersonmaterials.com. 2020. SEM Illustrative Example: Secondary Electron And Backscatter Electron Images | Anderson Materials Evaluation, Inc.. [online] Available at: <http://www.andersonmaterials.com/sem/sem-secondary-backscatter-images.html> [Accessed 24 May 2020].

[34] Bunaciu, A., Udriştioiu, E. and Aboul-Enein, H., 2015. X-Ray Diffraction: Instrumentation and Applications. Critical Reviews in Analytical Chemistry, 45(4), pp.289-299.

[35] Černík, M. and Thekkae Padil, V., 2013. Green synthesis of copper oxide nanoparticles using gum karaya as a biotemplate and their antibacterial application. International Journal of Nanomedicine, p.889.

[36] BraggsLaw. (2020). Retrieved 4 August 2020, from https://serc.carleton.edu/research$_e$*ducation/geochemsheets/BraggsLaw.html*

[37] GDOES Theory - Spectruma Website (english). Spectruma.de. (2020). Retrieved 16 August 2020, from https://www.spectruma.de/en/gdoes-theory.html.

[38] Nunez, A., 2019. High Temperature Corrosion In Exhaust Application For Heavy-Duty Trucks. Master thesis. KTH Royal Institute of Technology.

[39] L. Niewolak, D. J. Young, H. Hattendorf, L. Singheiser, and W. J. Quadakkers. Mechanisms of oxide scale formation on ferritic interconnect steel in simulated low and high po 2 service environments of solid oxide fuel cells. Oxidation of metals, 82(1-2):123–143, 2014.

[40] A.M. Huntz, A. Reckmann, C. Haut, C. Severac, M. Herbst, F.C.T. Resende, A.C.S. Sabioni, Oxidation of AISI 304 and AISI 439 stainless steels, Mater. Sci. Eng. A, 447 (2007) 266-276.

A

Appendix 1

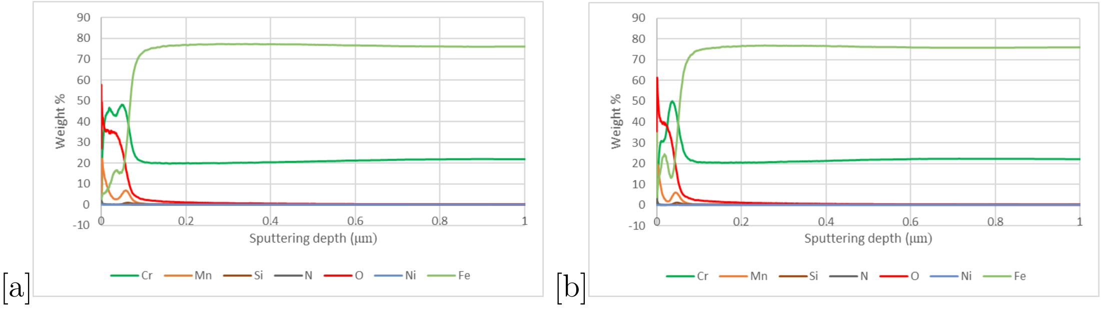

Figure A.1: Depth profile of 1.4622 a.) without ammonia ,b.) with ammonia

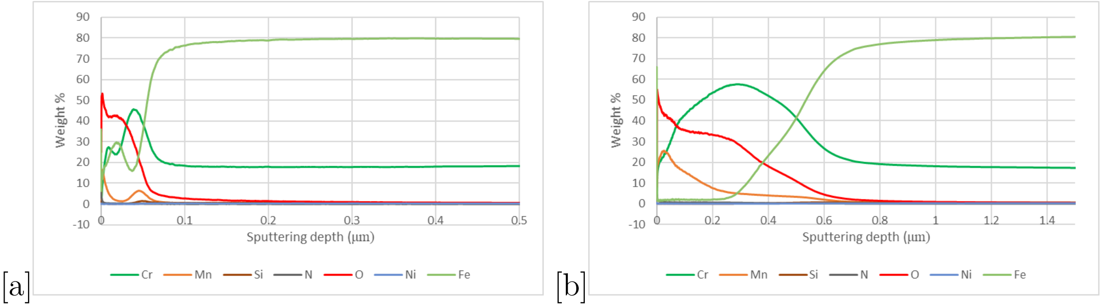

Figure A.2: Depth profile of 1.4509 a.) without ammonia ,b.) with ammonia

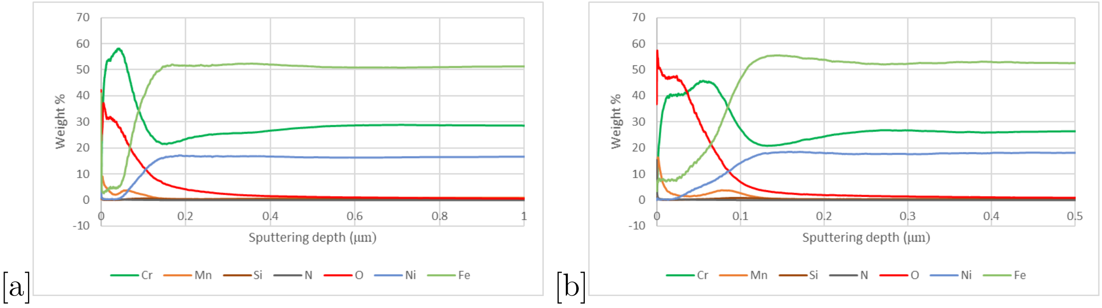

Figure A.3: Depth profile of 1.4951 a.) without ammonia ,b.) with ammonia

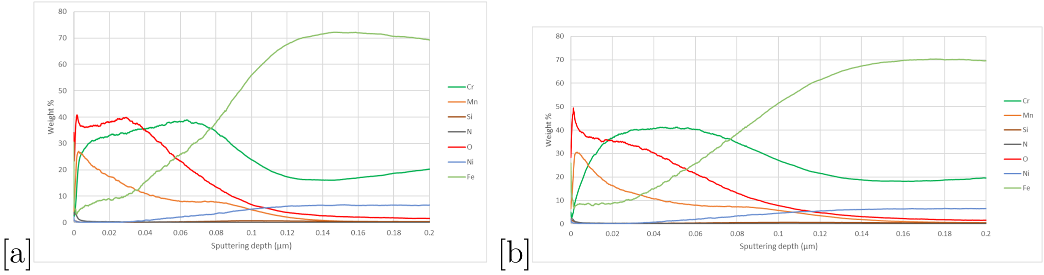

Figure A.4: Depth profile of 1.4307 a.) without ammonia ,b.) with ammonia

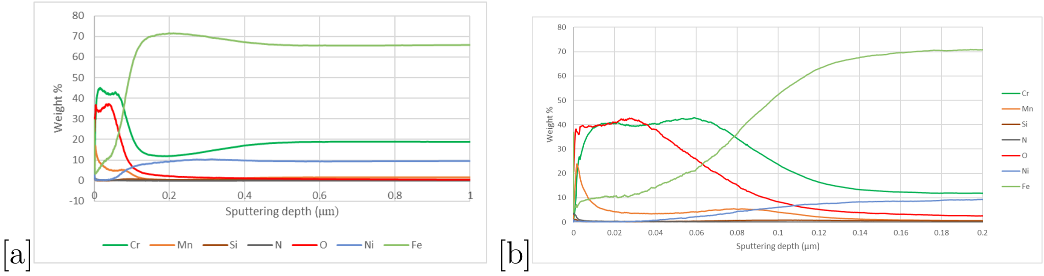

Figure A.5: Depth profile of 1.4404 a.) without ammonia ,b.) with ammonia

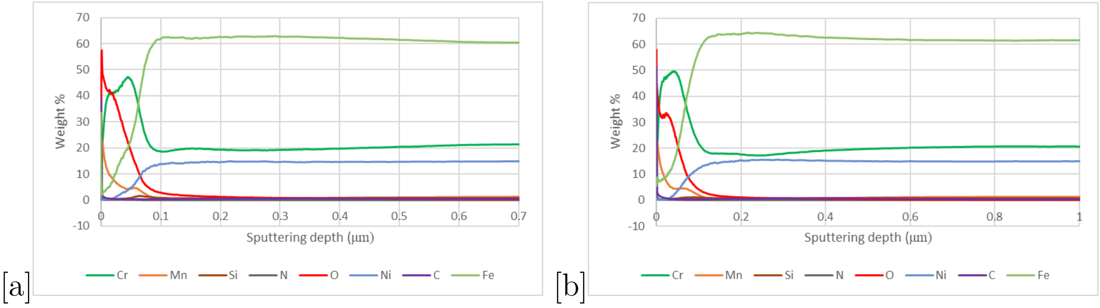

Figure A.6: Depth profile of HK30 a.) without ammonia ,b.) with ammonia

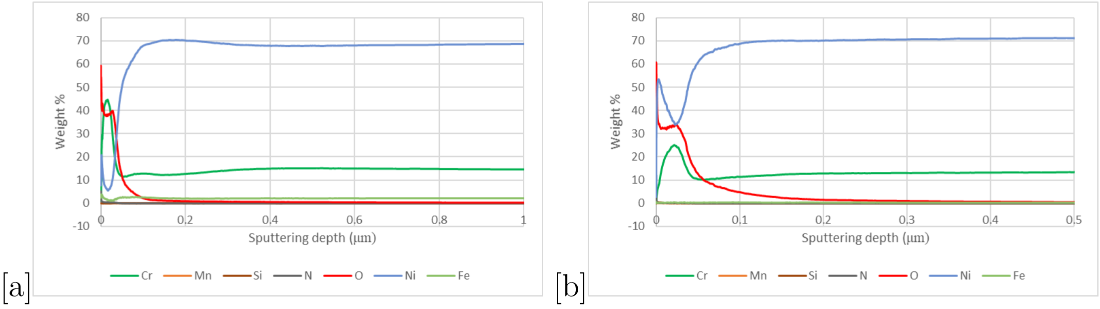

Figure A.7: Depth profile of 713C a.) without ammonia ,b.) with ammonia